NLTH and NLPO analyses of Building A
Module 3 – Harmonisatie berekeningsmethode

Longo, M.; Singla, A.; Messali, F.

Publication date
2020

Document Version
Final published version

Citation (APA)
Longo, M., Singla, A., & Messali, F. (2020). *NLTH and NLPO analyses of Building A: Module 3 – Harmonisatie berekeningsmethode*. Delft University of Technology.

Project number	CM1B13
File reference	CM1B13-R02
Date	19 October 2020
Corresponding author	Francesco Messali (f.messali@tudelft.nl)

Module 3 – Harmonisatie berekeningsmethode

NLTH AND NLPO ANALYSES OF BUILDING A

Authors: Michele Longo, Anmol Singla, Francesco Messali

***Cite as**: Longo, M., Singla, A., Messali, F. NLTH and NLPO analyses of Building A - Module 3 – Harmonisatie berekeningsmethode. Report no. CM1B13-R02, Version 03, 19 October 2020. Delft University of Technology*

This research work was funded by y Stichting Koninklijk Nederlands Normalisatie Instituut (NEN) under project number 8505400024-001.

Table of Contents

1 INTRODUCTION

This report summarizes the results for the numerical analyses of the detached house Building A in support to the development of NPR 9998 Module 3.

The following analysis types are carried out:

1. Non-linear pushover (NLPO) "full FEM"[1] analyses for uniform load distribution;
2. Non-linear time history (NLTH) "full FEM" analyses;
3. Simplified Lateral Mechanism Analyses (SLaMA), described and discussed in a separate document.

The following assumptions are considered:

- Backbone curves of piers and spandrels defined according to NPR 9998;
- Global and local acceptance criteria based on Annex G of NPR 9998;
- Indirect compliance assessment method as defined in Annex F of NPR 9998;
- Fixed based boundary conditions;
- Spectrum according to the Webtool.

The NLTH analyses consider both the original site-specific input ground motion, and a scaled ground motion.

For the sake of simplicity, where the following text refers to an article, a section or an Annex "of NPR", this is in fact referring to NPR 9998 [2].

1.1 Analysis Method

Both the NLPO and NLTH analyses were carried out using the non-linear finite element analysis program DIANA FEA, version 10.3. The building was modelled in 3D using shell and beam elements. For the masonry material, a non-linear orthotropic total strain based model was used, which is able to reproduce cracking, crushing and shear behaviour of masonry [1]. The materials of the concrete floors, including the rebars, were also modelled as non-linear. Elastic properties of the timber floor and were taken from calibrated parameters based on similar laboratory experiments. Roof structure is also modelled as linear elastic. Further details on the DIANA modelling approach are provided in Section 2.1.

1.2 NPR 9998 Acceptance Criteria

Both global and local acceptance criteria are considered. Global criteria are applied to the building as a whole and to the associated capacity curve. Local criteria are applied to specific elements, such as piers and spandrels.

1.2.1 Global acceptance criteria

The exceedance of the NC limit state is defined in Section G.6.1 of NPR. This occurs when:

- The total lateral force resistance has reduced by 50% relative to the maximum value.
- A number of load-bearing elements has exceeded its displacement capacity leading to partial or full building collapse.
- The drift limits defined according to table G.2 of NPR are exceeded.
- An Out-Of-Plane displacement of 60 mm is detected. This is in accordance with Annex H of NPR, as also recommended in section F.6.3 of NPR.

Other global criteria referred to the diaphragms are given in article G.9.5.2(2) of NPR.

1.2.2 Local acceptance criteria

The local acceptance criteria for piers are considered as recommended in sections G.9.2.2 and G.9.2.3 of NPR.

[1] As defined in Annex G of NPR 9998.

As regards the masonry spandrels, these are assumed not to be essential to the stability of the load-bearing system. Therefore, a maximum drift of 2% is assigned to rectangular spandrels. This is in accordance with section G.9.3.1(8) of NPR, and applies to both non-load bearing and load-bearing spandrels.

1.3 Boundary Conditions

The Building A is evaluated without considering the soil-structure interaction (SSI) effects, and a fixed based analysis is performed.

2 MODEL DESCRIPTION AND INPUT DATA

2.1 Building Overview and Modelling Approach

Building A is a two-storey (plus attic) detached house, built in 1996. The building is made of unreinforced masonry (URM) cavity walls. Additionally, an one-storey building appendix representing the garage is part of the structure. A picture and a plane section of the building is shown in Figure 1. Summary information about the building information is provided in Table 1.

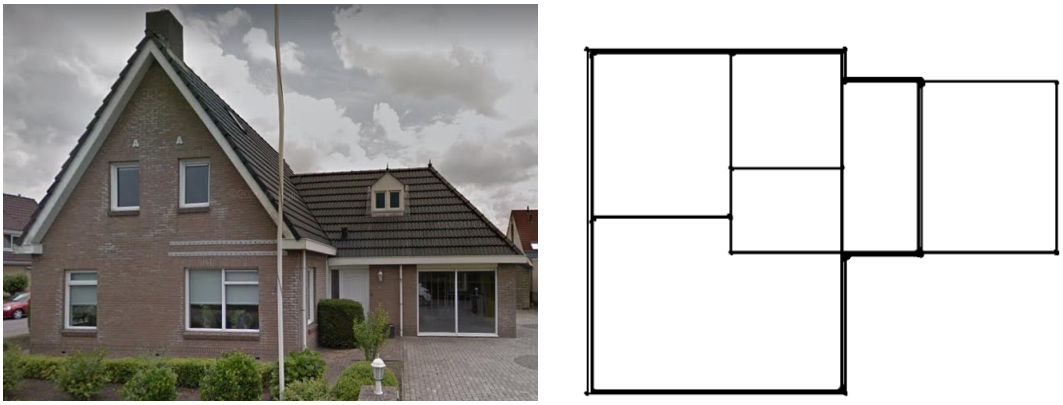

Figure 1. Building A detached house.

Table 1. Building A – Summary of the model building information.

Building year	1996
Number of storeys	2 plus attic
Height	7.91 m
Walls	Cavity wall system with wall ties (with density 6 /m^2): - Outer leaf: Clay brick - Inner leaf: CaSi brick Internal walls: - Load bearing: CaSi and Clay brick
Floors	Ground floor: Precast Prestressed Concrete T-Beams 1st floor: Main - Precast Reinforced Concrete Panels. Garage – Timber beams spanning X direction with chipboard panels 2nd floor (attic): Timber beams spanning Y direction with chipboard panels
Roof	Timber beams spanning Y direction with prefabricated Unidek panels
Roof-to-wall connection	Timber roof beams have a friction connection to the supporting walls. Friction acts in the wall out-of-plane direction.
Floor-to-wall connection	Ground Floor: Connected directly to the walls. 1st floor: In-plan (perpendicular to gravity) friction defined between floor and wall below. Floor connected directly to walls above. 2nd floor (Attic): Timber beams have a friction connection to the supporting walls. Friction is acting in the wall out-of-plane direction.
Floor-to-roof connection	Roof panels are nailed to wood ledger bolted to the top of the exterior masonry cavity walls.
Total mass	150 t
Footprint area	98 m^2
Material properties	Properties adopted for the unreinforced masonry walls assuming clay brickwork (post-1945) for the outer leaf and CaSi brickwork (1960-present) for the inner leaf properties – see Appendix A1

The detached house representing the Building A is numerically modelled in 3D by the software Diana 10.3. Since the garage part and the inner wall of the main building are not directly interconnected, as well as the floors, the garage is not modelled. A representation of the model is shown in Figure 2.

The cavity wall system is implemented by explicitly modelling the inner leaf and considering the outer leaf as dynamic mass acting in the direction perpendicular to the wall. The assumption in this case is that the wall ties are not able to transfer any force in the shear direction. The mass density assigned to the different

external walls is depicted in Figure 3. All the internal walls are explicitly modelled. All internal walls of both ground and first floor are not load bearing and thus they are disconnected from the top floor. No force is then transferred to the walls at that location. Wall to wall connection made by a vertical mortar joint, is modelled with a strip of weak elements that simulates the lack of interlocking between the two walls. An overview of the walls modelled with this technique is shown in Figure 4. Both internal and external walls are modelled using the Engineering Masonry Model [1]. The weak elements representing the connection are also modelled with the Engineering Masonry Model, but rotating the local axes and with both elastic and nonlinear properties reduced by 30%.
The ground precast prestressed concrete floor and the hollow core slab at the first floor are modelled as non-linear elements, considering the Total Rotating Strain Crack Model for concrete. The steel reinforcement is modelled as discrete or continues reinforcement using the Von Mises Plasticity model (Figure 5).
In order to include on the external façades the separation between masonry piers at different storey, rigid floor strips with the height equal to the concrete floor thickness, are modelled. A linear elastic isotropic material is assigned to such elements (Figure 6). The lintels are also modelled as linear elastic material.
The roof purlins, struts, ties and ridge beam are modelled with beam elements using a linear elastic isotropic material (Figure 7). The timber boards, representing the second floor diaphragm, are modelled as shell elements using linear elastic orthotropic material. The prefabricated Unideck panels, representing the roof structure, are modelled with linear elastic orthotropic material with negligible stiffness (Figure 8).

Quadratic 8-noded curved shell elements (CQ40S and CT30S) are used to model the walls, floors and lintels of the 3D building. The timber beams at the second floor and at the roof level are modelled with Class-III beam element (CL18B). The model is assumed to be fixed base (no soil-structure interaction is considered), so that it is fully restrained at the bottom from translations and rotations. The elements are meshed with an average size of 200x200 mm (Figure 2).

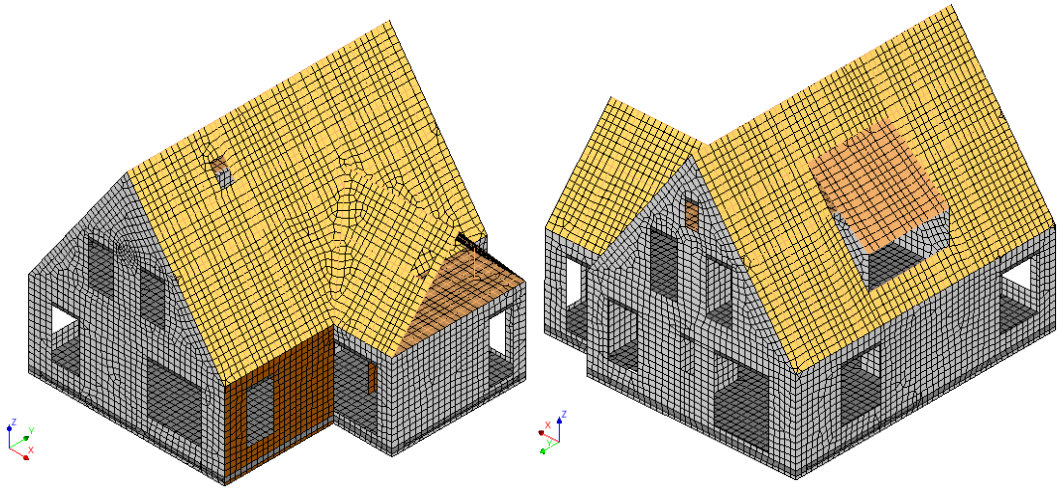

Figure 2. Diana Model of Building A.

Non Linear Pushover (NLPO) and Non Linear Time History (NLTH) analyses are conducted. For the NLPO analyses, the model is initially subjected to the gravity loads applied in ten equal steps. Then, either uniform distributed lateral loads, applied via a uniform lateral acceleration, or modal distributed lateral loads, based on the main eigen-mode of the structure (and the corresponding participating mass) obtained via eigen-value analyses, are applied so that an average displacement rate of 0.1 mm/step is recorded at floor level. It should be noted that the uniform lateral acceleration does not account for the extra dynamic mass. The Secant BFGS (Quasi-Newton) method is adopted as iterative method in combination with the Arc-Length control. Both displacement and force norms must be satisfied during the iterative procedure within a tolerance of 1%. For the NLTH analyses, the model is first subjected to gravity loads, again applied in ten equal steps. Then, the different acceleration motions are applied in the longitudinal, transversal and vertical direction at the base nodes, using a time step of 2.5 milliseconds. A Rayleigh damping of 2% is accounted in the calculation. The

Secant BFGS (Quasi-Newton) method is employed as iterative method. Energy norm must be satisfied during the iterative procedure with a tolerance of 0.01%. For both analyses, the Parallel Direct Sparse method is employed to solve the system of equations. The second order effects are considered via the Total Lagrange geometrical nonlinearity.

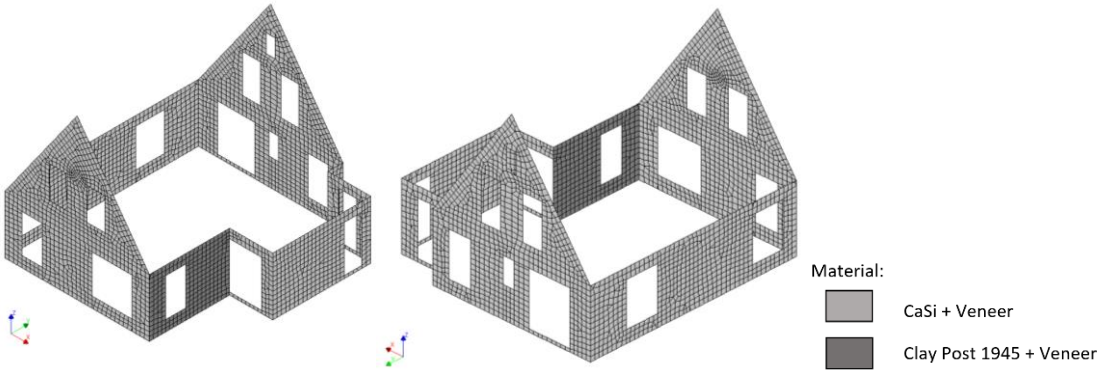

Figure 3. External walls material.

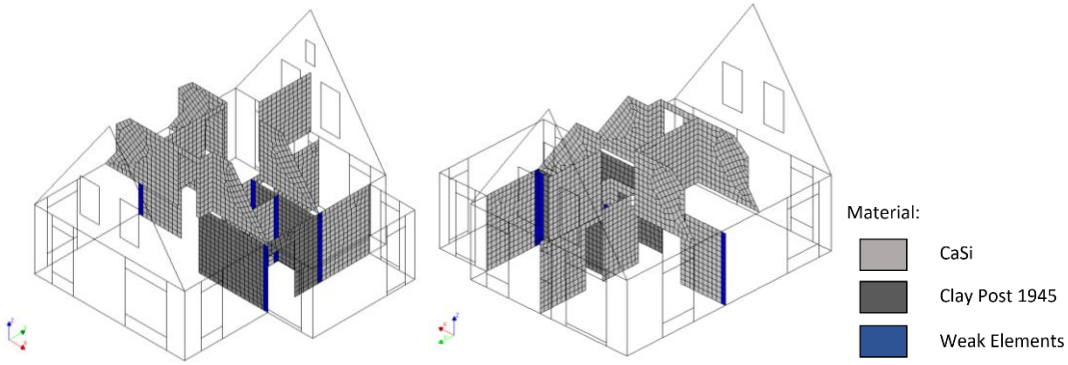

Figure 4. Internal walls material. Weak element connection is highlighted in blue.

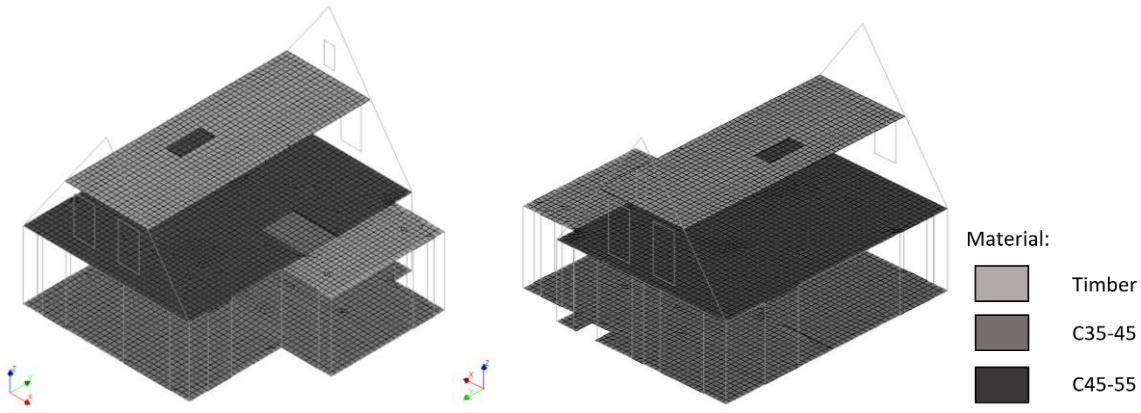

Figure 5. Floor material.

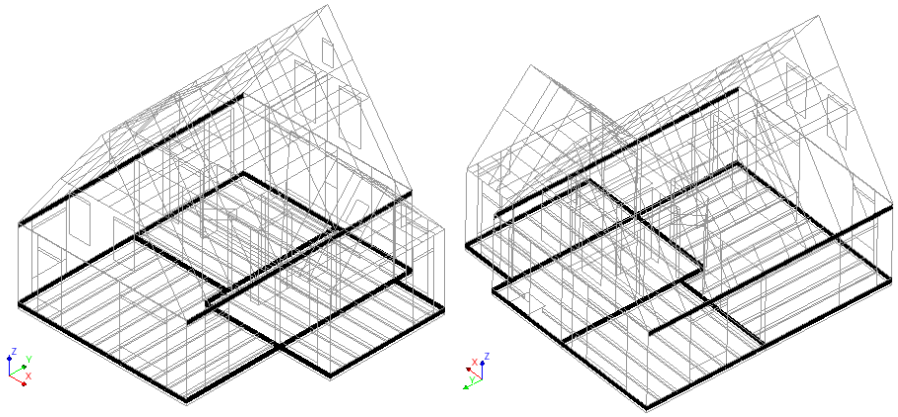

Figure 6. Concrete strips as separation of external masonry at different storey.

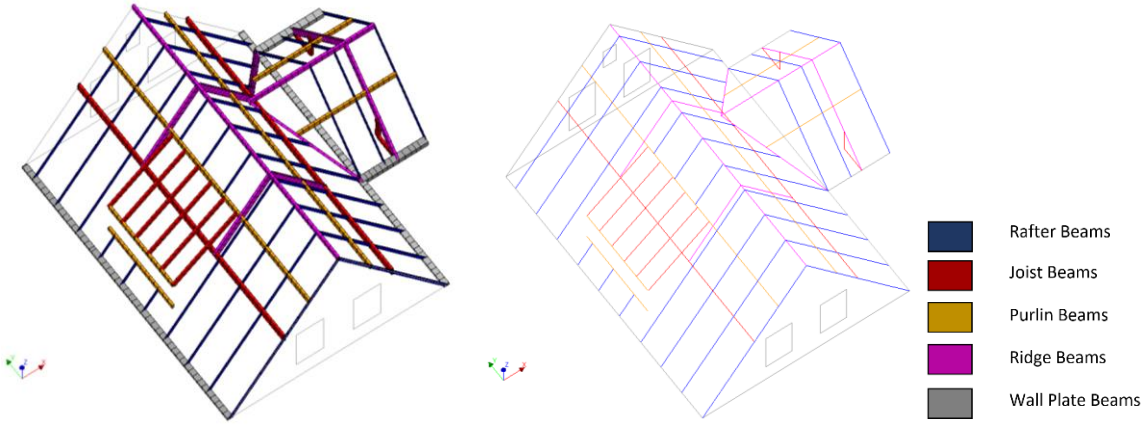

Figure 7. Roof beam structure.

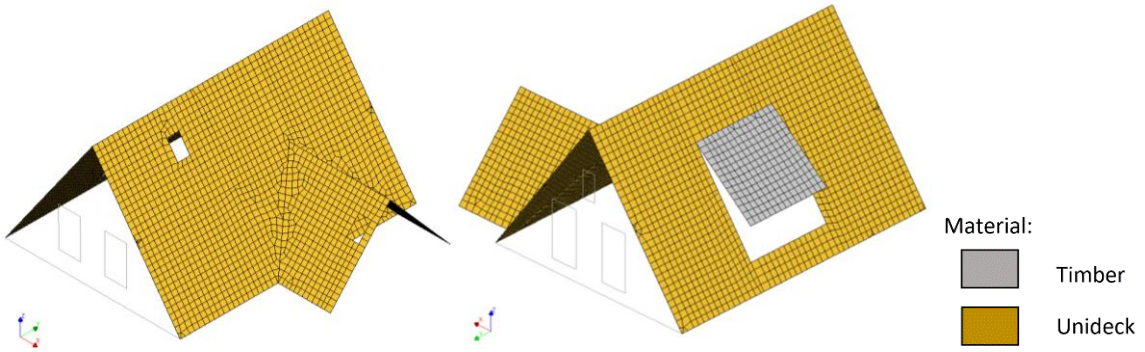

Figure 8. Roof boards.

2.2 Input Ground Motion and Spectrum

The surface level ground motions for the analyses are provided by the NEN web tool NPR 9998 [3]. For each ground motion, three components are provided (two horizontal and one vertical). The horizontal components x and y from the Web tool are aligned with the respective local x and y axes defined for the numerical models. In the case of "fixed base" boundary conditions, the surface level ground motions are applied directly to the base of the building and soil and foundation flexibility effects are not taken into account.
The information on the seismic inputs for the Building A model are summarised in Table 2.

The location of the Building A with respect to the ground motion clusters defined in the NEN web tool is shown in Figure 9. The elastic spectrum obtained from the web tool is shown in Figure 10.

Table 2. Building A: definition of seismic input.

Ground Motion Model	GMMv5 2018-10-01
Return period	2475 years
Time period	T1
Number of ground motions	11 (out of 11)
Ground motion cluster [3]	C
$a_g S$ (unscaled PGA) [3]	0.198g
Importance factor γ_1 [1] §2.2.3, Table 2.4	1
Scaling factor for number of GMs (11/11) with indirect check γ_n [1] §F.6.3	1
Scaling factor for number of GMs (11/11) with explicit check γ_n [1] §F.6.2	1.25

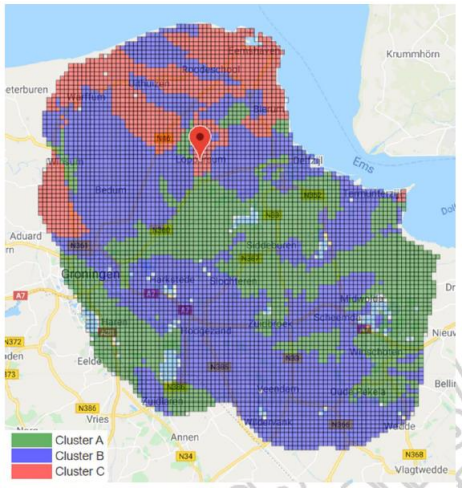

Figure 9. Building A: location of the building from Web tool NPR 2018 with ground motion clustering.

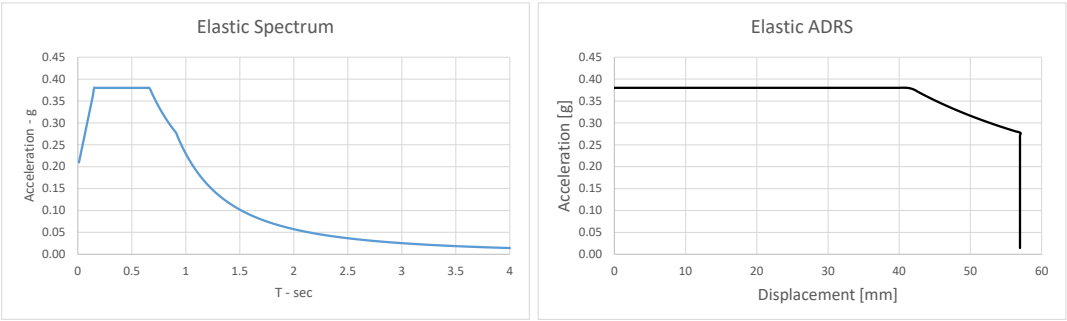

Figure 10. Building A: Elastic spectrum from web-tool.

2.3 Material Properties

The material properties of masonry are taken from Table F.2 of NPR. The masonry quality is considered as excellent [4]. Specific properties related to the Diana FEA material models are listed down below.

2.3.1 Masonry

Masonry is modelled using the Engineering Masonry Model [1]. The model consider the local axis y as the direction perpendicular to the bed joint and Poisson`s ratio equal to zero. The weak material assigned at the interface between internal non-loadbearing and external walls has rotated local axes and lower values of elastic and strength properties. For the NLTH calculations the elastic properties are halved in order to properly capture the cyclic strength degradation, not explicitly described by the EMM. Besides, the same assumption has been already employed in other calibration/validation studies of URM buildings to overcome the global rigidity given by local connections which results in over stiff results. An overview of the parameters employed in the material model is shown in Table 3. The NLTH material properties for the elastic parameters are included in parenthesis.

Table 3. Masonry properties numerical model. In parenthesis the values used for the NLTHA.

Engineering Masonry Model	CaSi	CaSi – Weak*	Clay	Clay – Weak*
E_y [MPa]	4000 (2000)	2800 (1400)	6000 (3000)	4200 (2100)
E_x [MPa]	2667 (1334)	1867 (934)	3000 (1500)	2100 (1050)
G [MPa]	1650 (825)	1155 (578)	2500 (1250)	1750 (875)
Density [Kg/m^3]	1850	1850	1950	1950
f_y [MPa]	0.15	0.10	0.30	0.21
Min f_x [MPa]	0.30	0.20	0.90	0.63
$G_{f,I}$ [N/m]	10	8.1	10	13.6
α [rad]	0.62	0.62	0.58	0.58
f_c [MPa]	7.0	7.0	10.0	10.0
G_c [N/m]	15000	15000	15000	15000
φ [rad]	0.54	0.57	0.643	0.643
c [MPa]	0.25	0.175	0.40	0.28
G_s [N/m]	100	100	200	200

* Rotated local axis

2.3.2 Timber Planks and Unideck

An orthotropic behaviour, whose properties are calibrated according to past laboratory experiment, is assigned to timber planks of the second floor. Unideck panels are also modelled with orthotropic behaviour, considering negligible stiffness. The local x axis is aligned with the global Y. The properties are tabulated in Table 4.

Table 4. Second floor timber diaphragm and Unideck Panels properties numerical model.

Linear Elastic Orthotropic	Timber C18 - Plates	Unideck
E_x [MPa]	1.5	10
E_y [MPa]	11	10
E_z [MPa]	400	10
Density [Kg/m^3]	380	-
υ [-]	0.15	0.00
G_{xy} [MPa]	1100	10
G_{yz} [MPa]	1100	10
G_{xz} [MPa]	500	10

2.3.3 Timber Beams

Beam properties are considered as isotropic linear elastic. The material assigned to purlins, rafters, joists, wall plates and ridge beams are listed in Table 5.

Table 5. Timber beam properties numerical model.

Linear Elastic Isotropic	Timber C18
E [MPa]	9000
Density [Kg/m^3]	380
υ [-]	0.35

2.3.4 Reinforced Concrete

Floor material is modelled as non-linear using the Total Strain Rotating Crack Model for the concrete and the Von Mises plasticity for the rebar. The properties are listed in Table 6 and Table 7.

Table 6. Reinforced concrete properties numerical model.

Total Strain Rotating Crack Model	C35/45	Hollow Core
E [MPa]	32643	27467*
Density [Kg/m^3]	2500	2000*
υ [-]	0.15	0.15
f_t [MPa]	2.25	2.65
$G_{f,I}$ [N/m]	138	145
f_c [MPa]	35.0	45.0
G_c [N/m]	34610	36211

*Computed value

Table 7. Rebar properties numerical model.

Von Mises Plasticity	Fe500	Fe1670	Fe1770
E [MPa]	200000	200000	200000
f_y [MPa]	500	1670	1770

2.4 Interstorey and Effective Heights

The interstorey height is shown in Figure 11. The effective height corresponds to the first floor height. The effective height and effective mass are listed in Table 8.

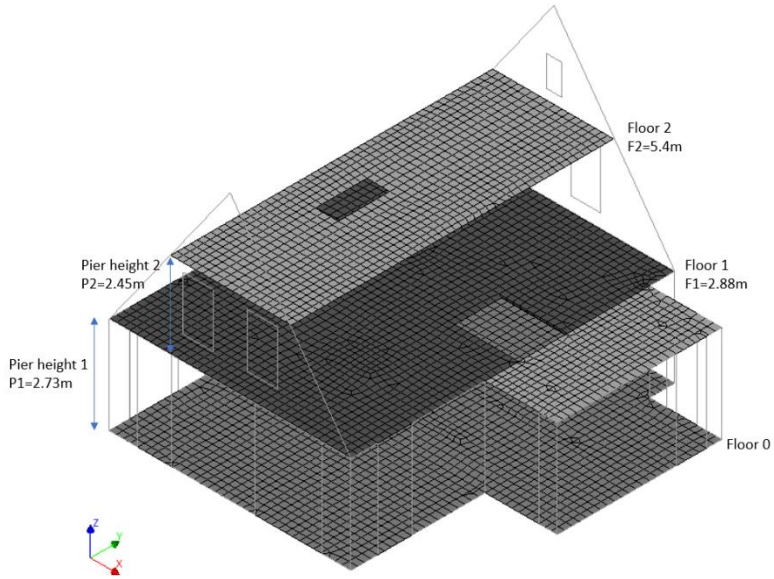

Figure 11. Floor height definitions.

Table 8. Effective height and effective mass.

Effective Height [m]	Effective Mass [ton]
2.88	74.4

2.5 Vertical Loads

The floor weights and the non-structural mass are given in Table 9.

Table 9. Floor weights and non-structural mass.

Models	Dead Load [kN/m²]	Superimposed Dead Load [kN/m²]	Live Load [kN/m²]	Comments
Ground – PS Isolatievloer	2.185	1.00	0.315	50 mm screed
Storey 1 – Kanaalplaatvloer	2.960	0.80	0.315	50 mm screed
Storey 1 – Timber	0.185	0.00	0.315	-
Storey 2 – Timber	0.185	0.00	0.315	-
Roof – Purlins, Trusses, Rafters	0.100	0.50	0.000	Tiles

2.6 Mass and Vertical Reaction

The static and dynamic mass for each floor is listed in Table 10. The dynamic mass includes the mass of veneers, and extra-floor-mass, as specified in Section 2.5.

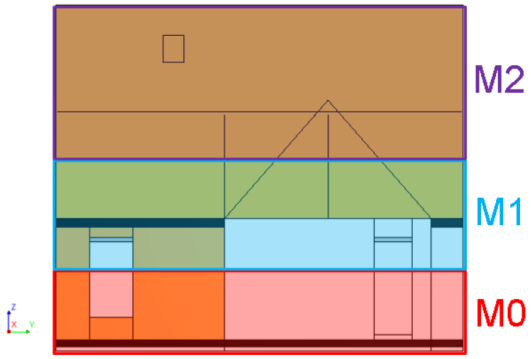

Figure 12. Mass division to the different storeys.

Table 10. Static and Dynamic Masses per each storey.

Mass	Static Mass [ton]	Dynamic Mass [ton]
M0	45.53	58.60
M1	43.76	56.30
M2	6.44	18.10
Mtot	**95.73**	**133.00**

The total vertical reaction force is equal to 940 kN corresponding to a total mass of 95.82 tons for the static mass. The dynamic mass accounted in the model is equal to 133.0 tons.

2.7 Element labelling

Piers, window banks and spandrels are labelled in order to assess their local behaviour in terms of load and displacement capacity. The name configuration consists of:

- A letter to indicate the element location: N for north façade, S for south façade, W for west façade, E for east façade, I for internal wall (either longitudinal or transversal).
- A letter to indicate the element type: P for pier, Ba for bank and Sp for spandrel.
- A number defining the level of the element: 1 for the element located between ground and first storey and 2 for the element located between first and attic storey level.
- A progressive number to univocally identify a specific element.

An overview of the labelling is shown in Figure 13 for piers and in Figure 14 for window banks and spandrels.

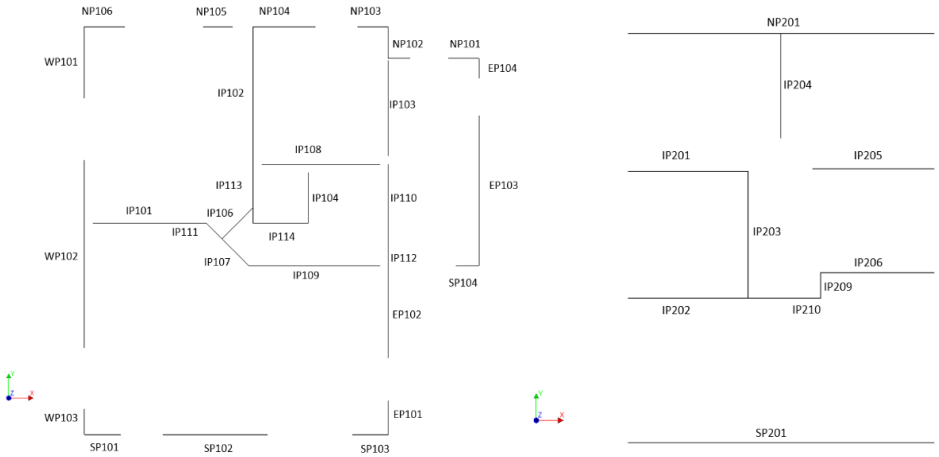

Figure 13. Pier labelling for ground and first floor.

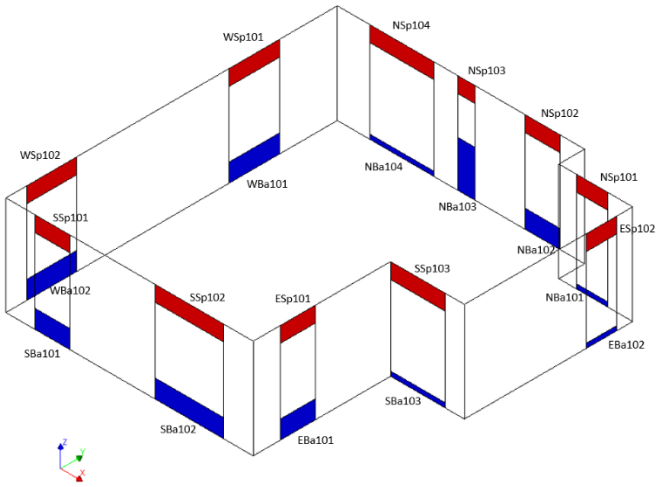

Figure 14. Banks and Spandrel labelling for ground floor.

2.8 Unknown Information and Modelling Assumptions

The model is based on the following assumptions/limitations:

- No structural drawings were available;
- The appendix is not modelled;
- No interaction between the building unit and the appendix is assumed;
- The veneer (outer leaves) is not modelled explicitly, rather as dynamic mass acting in the direction perpendicular to the wall;
- The connection between longitudinal and transversal walls (load-bearing) is consider as interlocked;
- Not interlocked connection between internal non-load bearing walls and load-bearing walls is assumed as weak connection, assigning low material properties to a strip of elements along the connection;
- No connection is considered between the internal non-load bearing walls and the floor above them;
- The connection between floors and walls is considered as fully fixed (they have same translations and rotations);

3 NLPO ANALYSES

3.1 NLPO Assessment

The Building A is assessed via Non-Linear Pushover Analyses with Diana FEA 10.3. Two different pushover load types are investigated:

- uniform distributed acceleration: the entire structure is subjected to a lateral acceleration.
- distributed floor load: a load proportional to the mass is evenly distributed at first and second floor level. The applied load is proportional to the mass of the specific floor.

The load is applied in both global X and Y direction.

3.2 Global Results

3.2.1 Failure Mechanisms

The failure mechanisms of the different analyses are reported below. In the analyses where the acceleration is applied, local failure occurs. In the Y direction, two-way OOP bending failure of the South façade at first floor level is detected for both positive and negative acceleration (Figure 15, Figure 16). The analysis suddenly diverges when the OOP displacement reaches about 50 mm. From a numerical point of view it can be interpreted as a collapse. When the load is applied in the X direction, the mechanism is concentrated in the partition wall located at the first floor connected to the North façade (Figure 19, Figure 20). The cantilever wall is rocking in its OOP direction. The analyses stop prematurely due to numerical instability.

A different failure mechanism is detected when the load is applied at floor level. For the load in Y direction, an in-plane failure is observed. The East façade is showing flexural behaviour, while the West façade is mainly characterized by shear failure. North and South façades show one-way OOP bending. From Figure 17, Figure 18 it's clear how torsion effects are taking place during the loading. The in-plane displacements are higher in the West façade. The East side displaces less due to the extra partition which provides extra stiffness. In direction X, both South and North façade (which are loaded in-plane) undergo shear failure. Flexural behaviour is detected in façades West and East. No torsion effect are detected. Results are shown in Figure 21 and Figure 22.

While for the NLPO with uniform acceleration load, the type of failure can be considered as OOP, in the NLPO with uniform load at the floor level, the detected failure is shear at ground storey. In the former an OOP limit of 60 mm is set. In the latter, the inter-storey drift limit is equal to 0.6% (related to brittle failure).

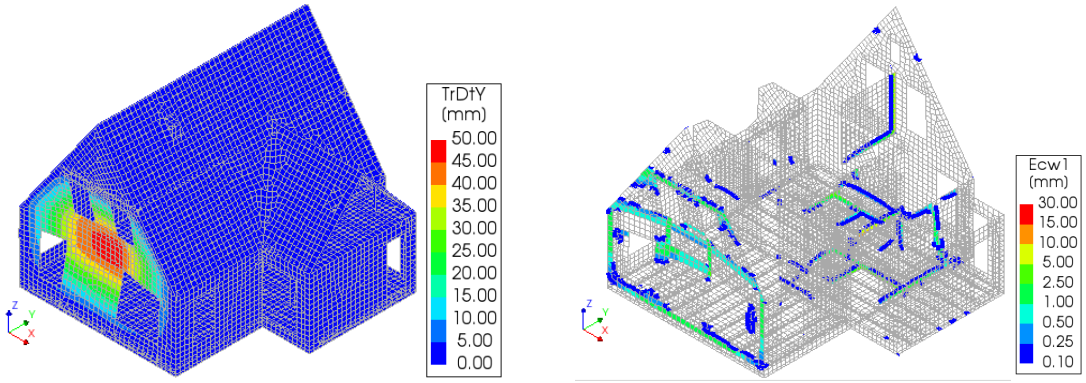

Figure 15. Uniform acceleration Positive Y direction. Displacement Y direction and principal crack width at step 235. Deformed mesh magnified 10 times.

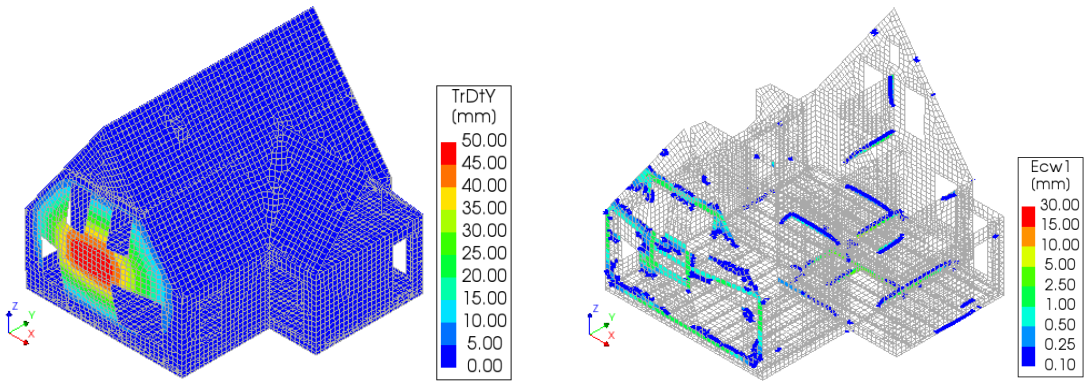

Figure 16. Uniform acceleration Negative Y direction. Displacement Y direction and principal crack width at step 235. Deformed mesh magnified 10 times.

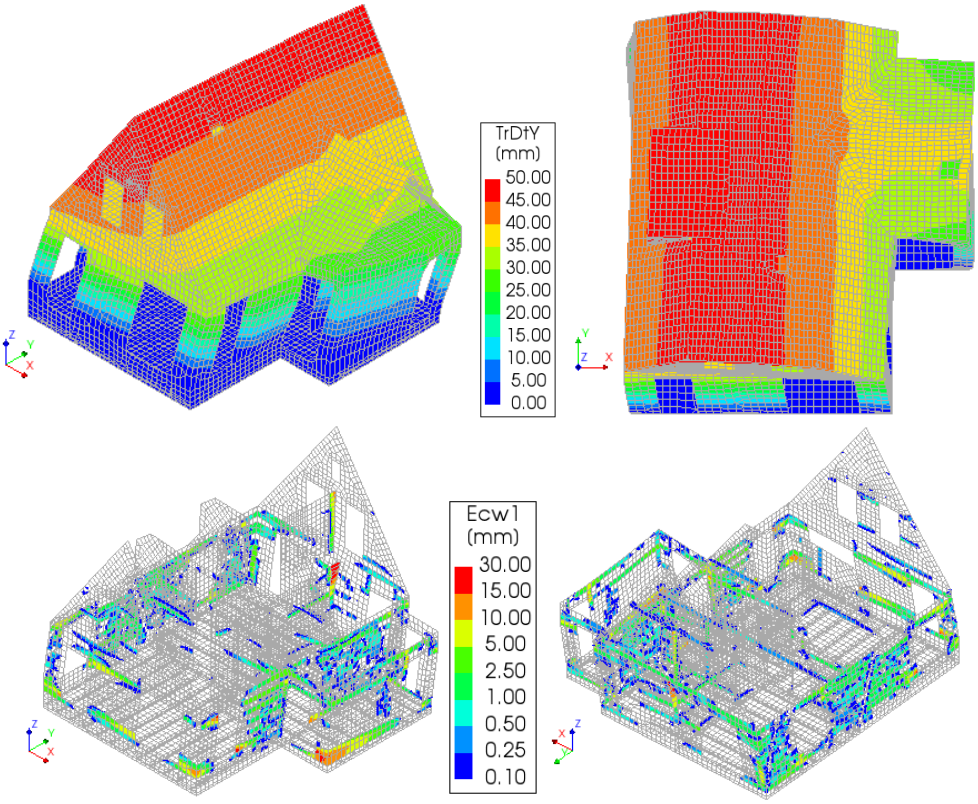

Figure 17. Distributed floor load Positive Y direction. Displacement Y direction at step 385. Principal Crack Width. Deformation Amplified 30 times.

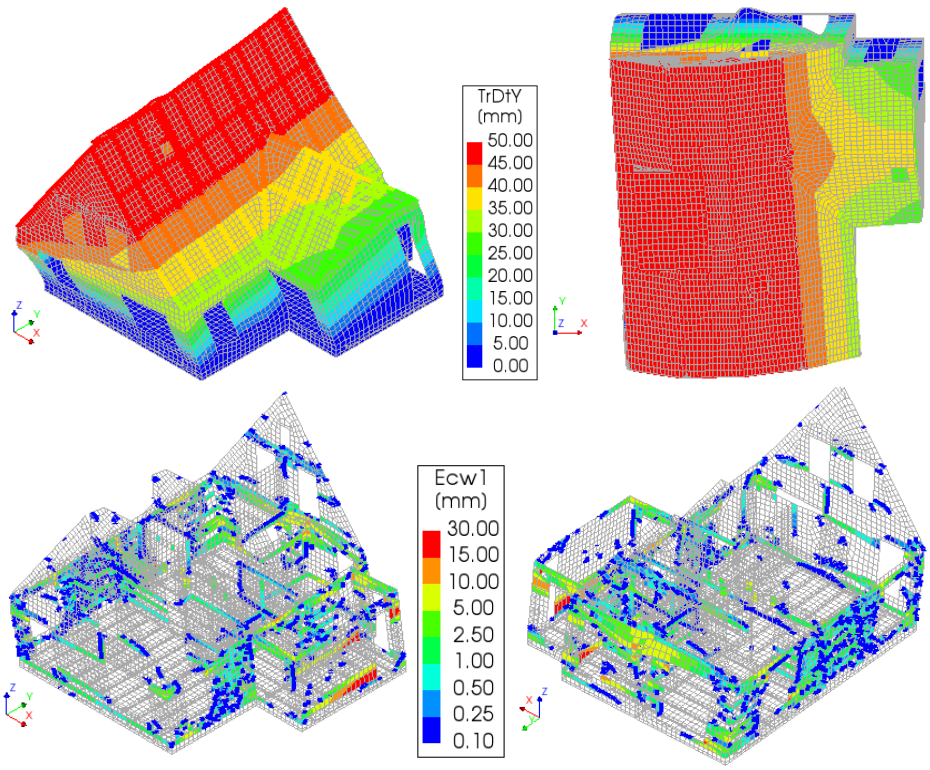

Figure 18. Distributed floor load Negative Y direction. Displacement Y direction at step 385. Principal Crack Width. Deformation Amplified 30 times.

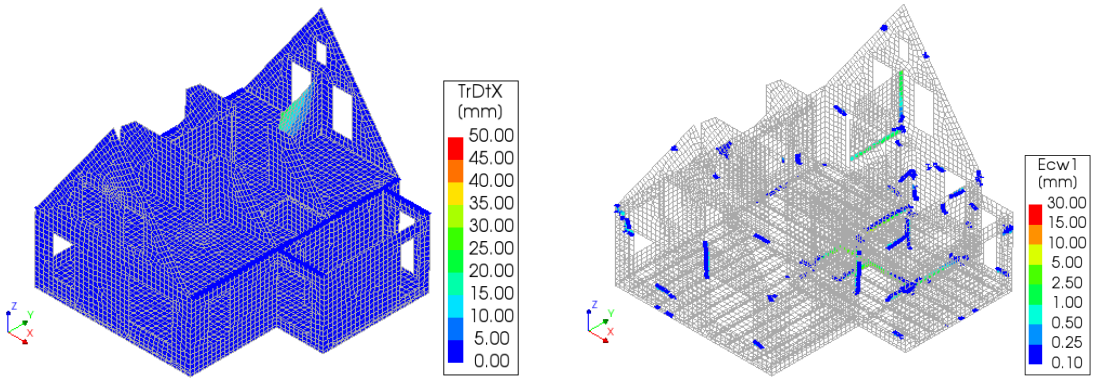

Figure 19. Uniform acceleration Positive X direction. Displacement X direction and principal crack width at step 110. Deformed mesh magnified 30 times.

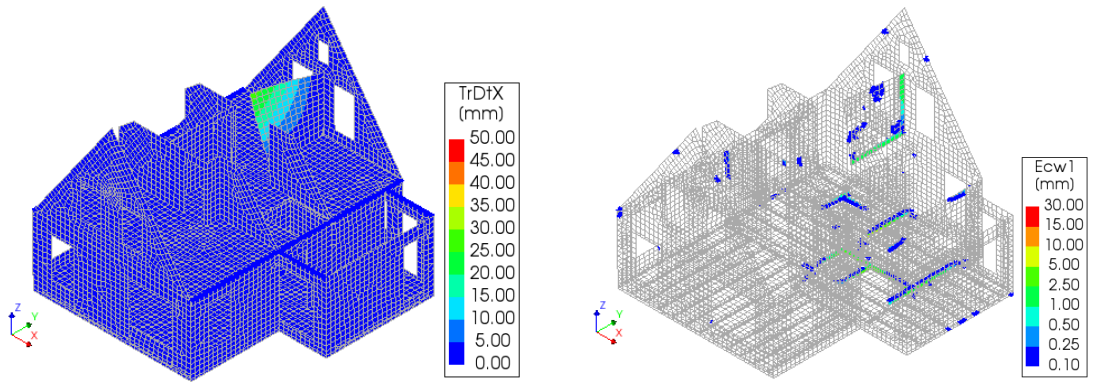

Figure 20. Uniform acceleration Negative X direction. Displacement X direction and principal crack width at step 110. Deformed mesh magnified 10 times.

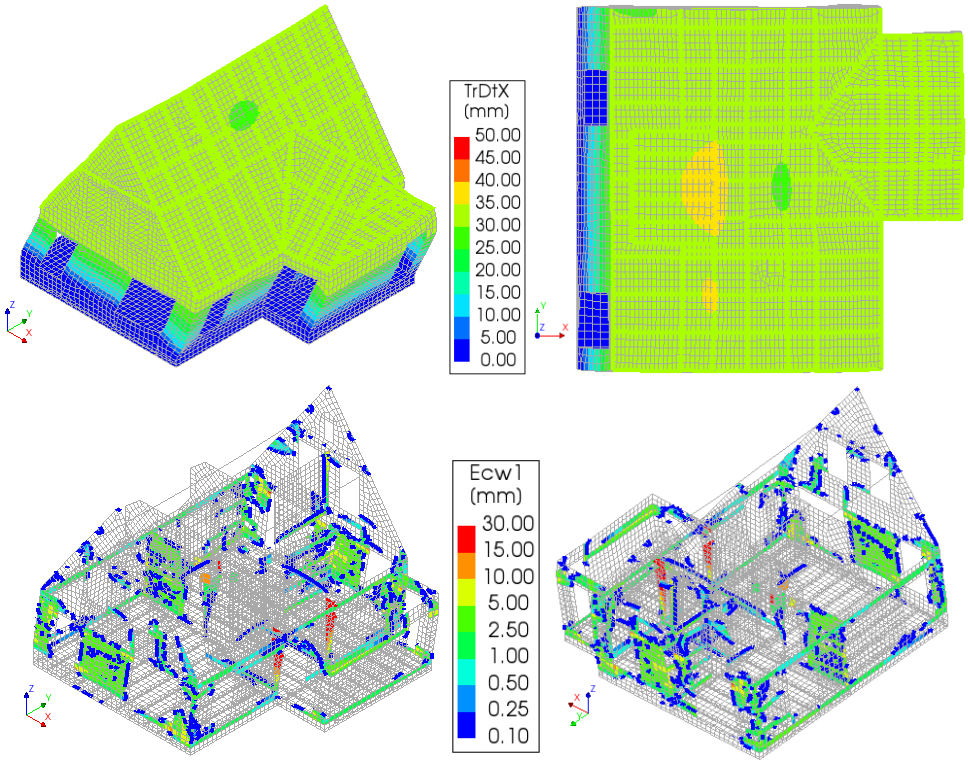

Figure 21. Distributed floor load Positive X direction. Displacement X direction at step 310. Principal Crack Width. Deformation Amplified 30 times.

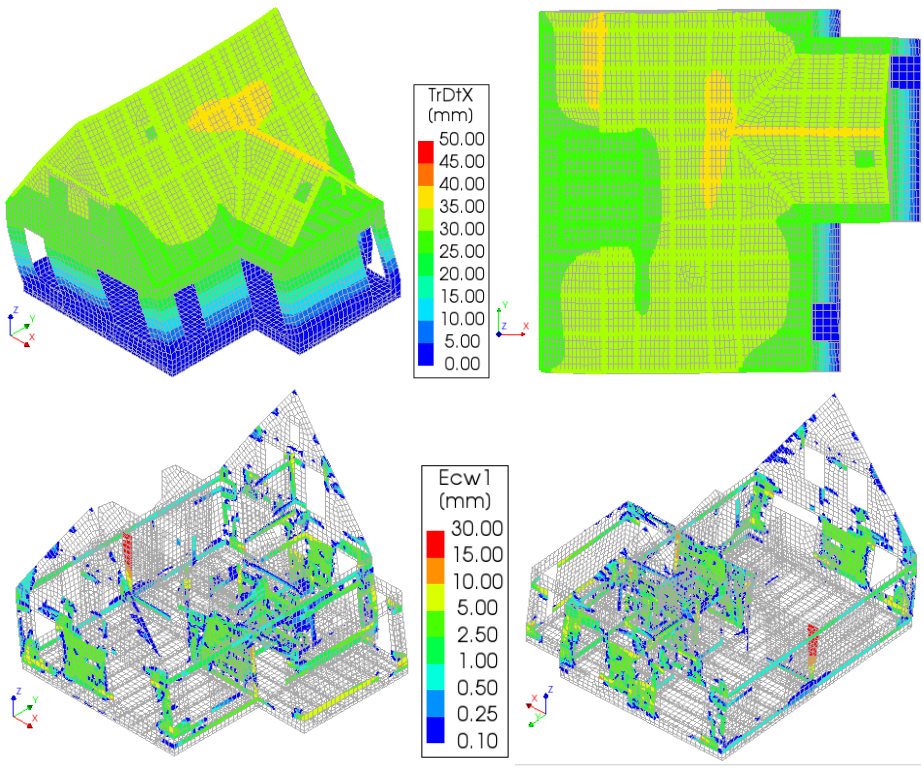

Figure 22. Distributed floor load Negative X direction. Displacement X direction at step 385. Principal Crack Width. Deformation Amplified 30 times.

3.2.2 Capacity Curves

The force-displacement and acceleration-displacement diagrams for the different analyses are shown from Figure 23 to Figure 27. The torsion effect correlated to the NLPO in y direction when pushed at floor level is plotted in Figure 26. It can be seen that at the end of the protocol the difference in displacement between East and West façade is about 10 mm. The vertical yellow line in Figure 25, Figure 26 and Figure 27 refers to the 0.6% drift limit of the ground floor. The acceleration is computed dividing the force by the effective mass. The force-displacement curves of the NLPO with floor load are then bilinearized following the procedure recommended in section G.4 and shown in Figure 28. The main results of both multilinear and bilinearized pushover curves are tabulated in Table 11 and Table 12.

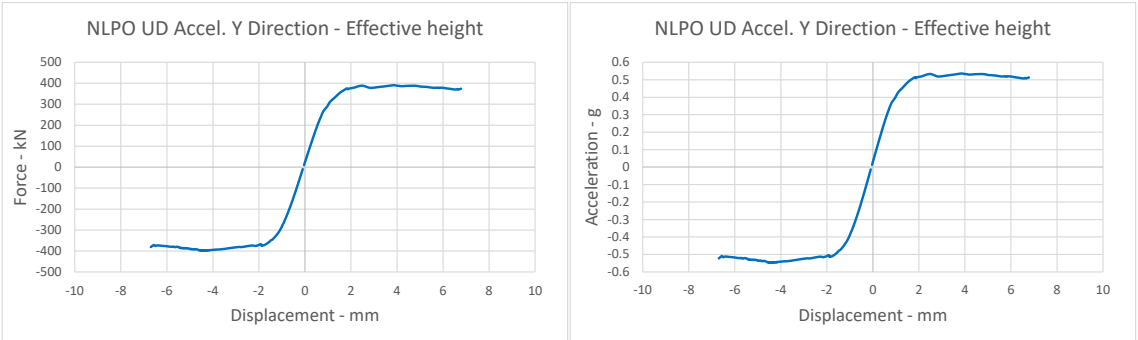

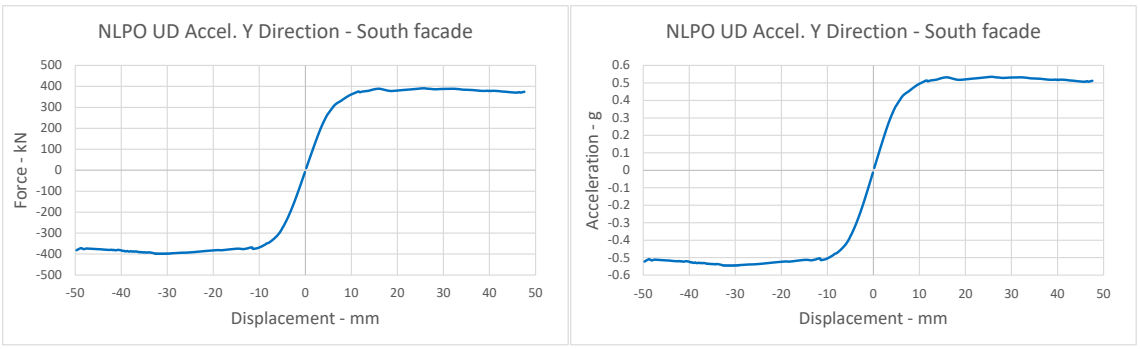

Figure 23. Uniform Distribution Acceleration Load, Y direction. Capacity curve related to effective height and South façade.

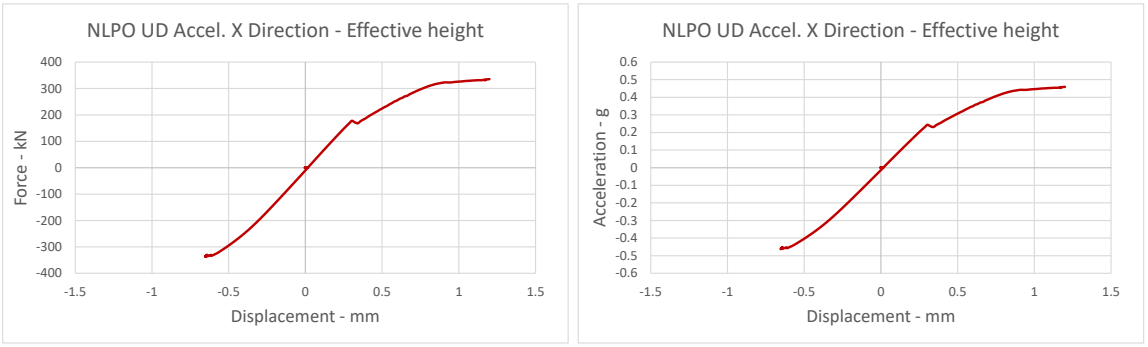

Figure 24. Uniform Distribution Acceleration Load, X direction. Capacity curve related to effective height.

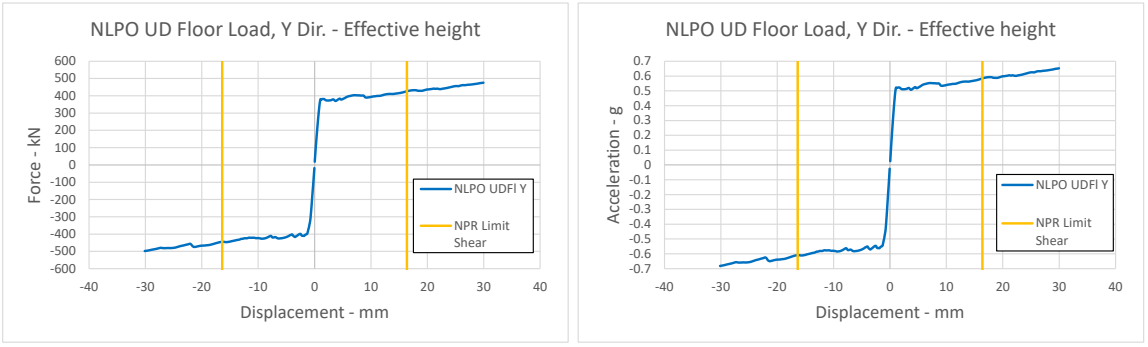

Figure 25. Uniform Distribution Floor Load, Y direction. Capacity curve related to effective height.

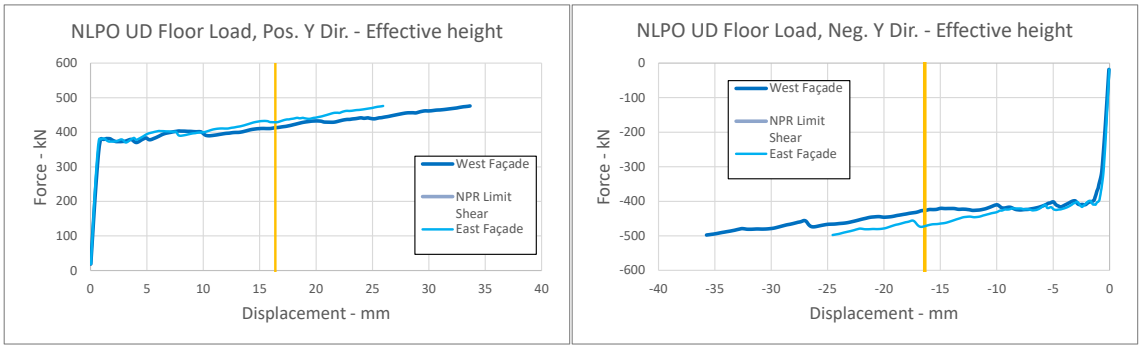

Figure 26. Torsion effect of Uniform Distribution Floor Load, Y direction. Capacity curve related to effective height.

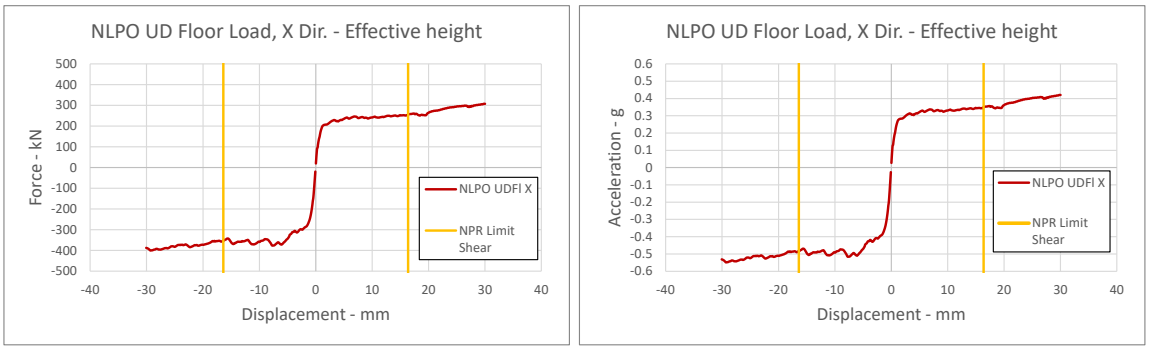

Figure 27. Uniform Distribution Floor Load, X direction. Capacity curve related to effective height.

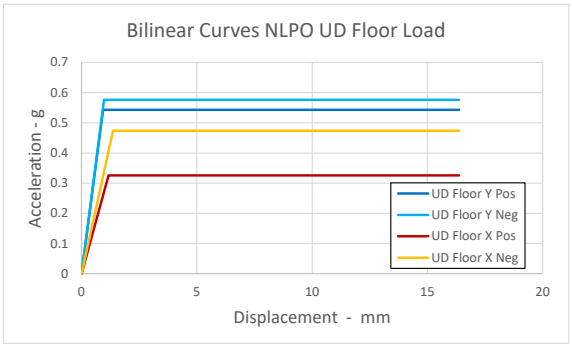

Figure 28. NLPO comparison. Bilinear Curves.

Table 11. Global NLPO Results.

Models	Governing Failure	Capacity [kN]	Acceleration [g]	Effective Height AVG Displacement [mm]
Uniform Acceleration – Positive Y	OOP South Façade	390.71	0.535	6.78
Uniform Acceleration – Negative Y	OOP South Façade	398.80	0.546	6.69
Uniform Acceleration – Positive X	-	335.42	0.460	1.20
Uniform Acceleration – Negative X	-	337.27	0.462	0.65
Uniform Floor Load – Positive Y	Shear	426.89	0.585	16.38*
Uniform Floor Load – Negative Y	Shear	444.82	0.610	16.38*
Uniform Floor Load – Positive X	Shear	251.02	0.344	16.38*
Uniform Floor Load – Negative X	Shear	352.28	0.483	16.38*

*NPR Limit for brittle failure

Table 12. Global NLPO Results – Bilinearized Curves.

Models	Yield Displacement [mm]	Displacement Capacity [mm]	Capacity [kN]	Acceleration [g]
Uniform Floor Load – Positive Y	0.932	16.38	396.46	0.543
Uniform Floor Load – Negative Y	0.972	16.38	420.52	0.576
Uniform Floor Load – Positive X	1.166	16.38	237.94	0.326
Uniform Floor Load – Negative X	1.369	16.38	345.62	0.474

3.2.3 Inter-storey Drifts

Inter-storey drift displacements are expressed in terms of drifts in Table 13.

Table 13. NLPO inter-storey displacement and drifts. Displacement/drift in Y direction are considered for the analysis with load applied in Y direction. Displacement/drift in X direction for the other two.

Models	Inter-storey drift Floor 1 [-]	Inter-storey drift Floor 2 [-]	Inter-storey drift Floor 3 [-]
Uniform Floor Load – Positive Y	16.38 mm / 0.60 %	7.17 mm / 0.28%	0.77 mm / 0.03%
Uniform Floor Load – Negative Y	16.38 mm / 0.60 %	5.86 mm / 0.23%	0.98 mm / 0.04%
Uniform Floor Load – Positive X	16.38 mm / 0.60 %	0.39 mm / 0.02%	0.57 mm / 0.02%
Uniform Floor Load – Negative X	16.38 mm / 0.60 %	2.00 mm / 0.08%	0.18 mm / 0.01%

3.2.4 Assessment

The assessment of the NLPO analyses where the load is uniformly applied at the floor location is made following the procedure described in Annex G of NPR. The pushover loaded in Y direction meet the capacity seismic demand for the elastic ADRS as shown in Figure 29. The elastic spectrum is scaled to the non-linear ADRS for the pushover loaded in X direction. The plot is shown in Figure 29. Value of global ductility and equivalent viscous damping are listed in Table 14.

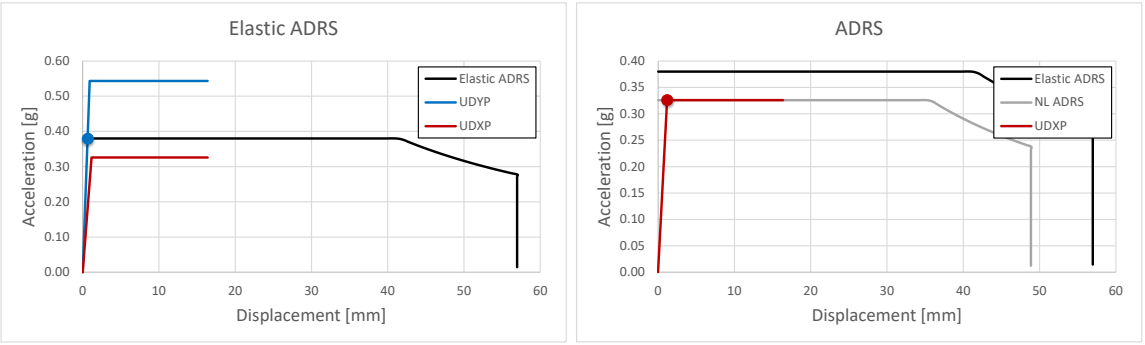

Figure 29. NLPO assessment. Elastic (left) and non-linear (right) ADRS for site-specific hazard.

Table 14. Uniform Floor Load NLPO X direction equivalent damping and global ductility for non-linear ADRS. ADRS for site-specific hazard.

Models	Equivalent Damping ξ_{sys}	Global Ductility μ_{sys}
Uniform Floor Load – Positive X	7.51 %	1.170

The site-specific PGA is then scaled in order to satisfy the demand of the pushover analyses for the non-linear ADRS. The iterated PGA of the pushover in the Y direction is equal to 0.501 g, while for the X direction is 0.301 g. The scaled ADRS plots together with the performance points are represented in Figure 30. In Table 15, the scaled PGA, global ductility and equivalent viscous damping are listed.

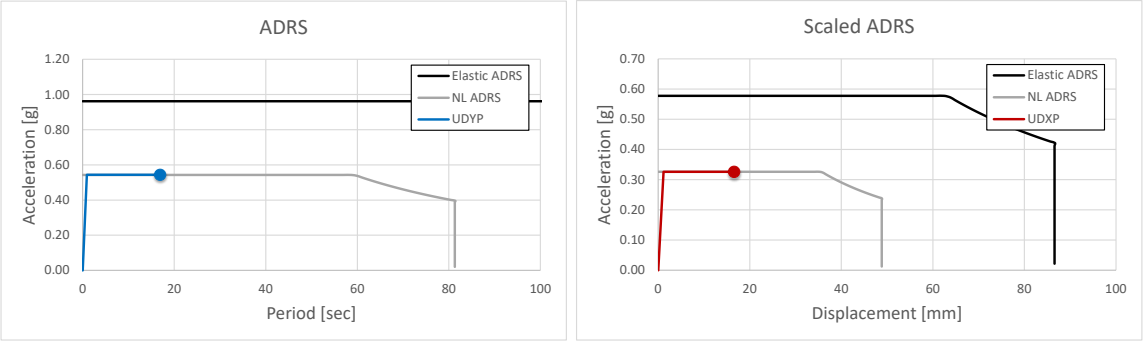

Figure 30. NLPO assessment. Scaled ADRS for positive Y load direction (left) and positive X load direction (right).

Table 15. NLPO equivalent damping and global ductility for non-linear scaled ADRS.

Models	Scaled Acceleration [g]	Equivalent Damping ξ_{sys}	Global Ductility μ_{sys}
Uniform Floor Load – Positive Y	0.501	20.00%	17.58
Uniform Floor Load – Positive X	0.301	20.00%	14.04

4 NLTH ANALYSES

4.1 NPR Assessment For Site-Specific Hazard – Indirect Method

The site-specific hazard is assessed using the indirect method as defined in section F.6.3 of NPR. The ground motions input is described in Section 2.2.

The main natural mode is shown in Figure 31, which show the OOP mechanism of the South façade. The main eigen-frequency is equal to 3.6634 Hz which gives a period of 0.273 s.

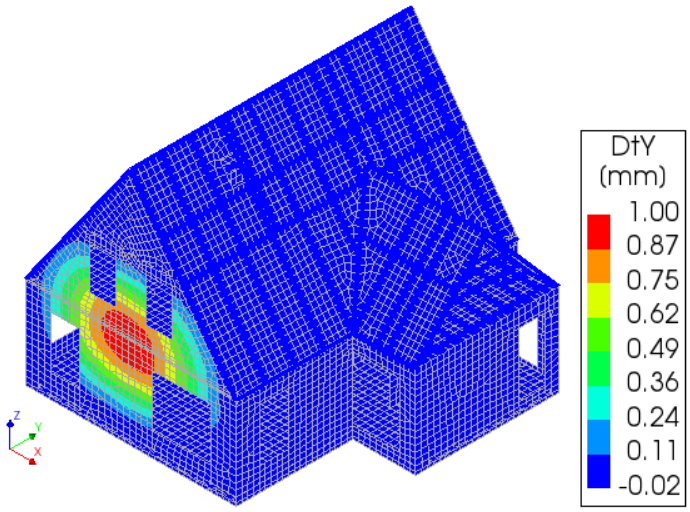

Figure 31. First natural mode of Building A. Displacement Y direction.

Overall, the Building A complies with NPR. The average maximum inter-storey displacement in x direction is recorded at the first floor location and equals to 1.24 mm, equal to 0.05% drift. The average maximum inter-storey displacement in the y direction reaches 3.41 mm, equal to 0.14% of drift. It is located at the ridge level. The OOP displacement at the South façade reaches an average of 22.63 mm. The average peak forces are equal to 198.3 kN in the positive direction and 240.8 kN for the negative direction in x. For the y direction the maximum forces in positive and negative direction are 211.3 kN and 211.9 kN.

4.1.1 Failure Mechanisms

The observed failure mechanism is a two-way OOP bending failure at the first storey level of the South façade. A displacement limit of 60 mm is considered for the OOP failure. An example of failure mechanism is reported below in Figure 32 and Figure 33.

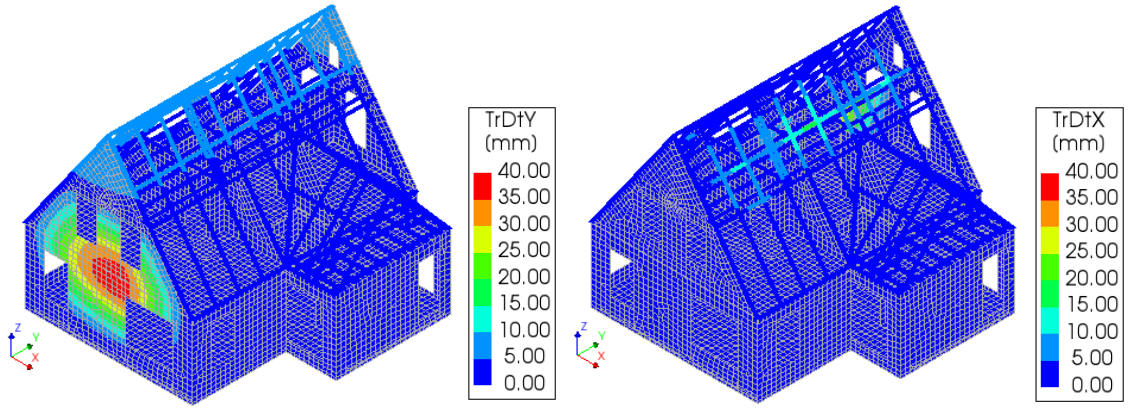

Figure 32. GM ID 3 for site-specific hazard. Absolute maximum displacement in Y (left) and X (right) direction recorded during the entire motion.

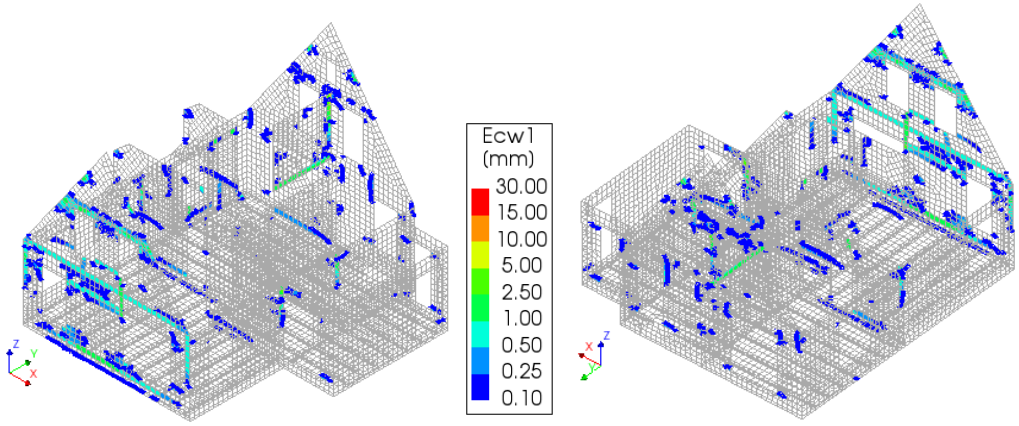

Figure 33. GM ID 3 for site-specific hazard. Absolute maximum principal crack width recorded during the entire motion. South-East (left) and North-West (right) view.

4.1.2 Inter-storey Drifts

In order to check the drift/displacement limit, different results of inter-storey drift/displacement are computed:

- Floor Displacement: as average of six nodes of hollow-core slab and timber floor (four corners and mid-point West and East side) and average of two nodes of ridge beam.
- Average Storey Displacement: as average of hollow-core floor displacement (see above) plus two nodes, respectively at South and North façade (floor height).
- OOP Displacement: displacement in y direction South and North façade (floor height).

Output point locations of the first floor are shown in Figure 34, while the output locations of timber floor and roof are shown in Figure 35.

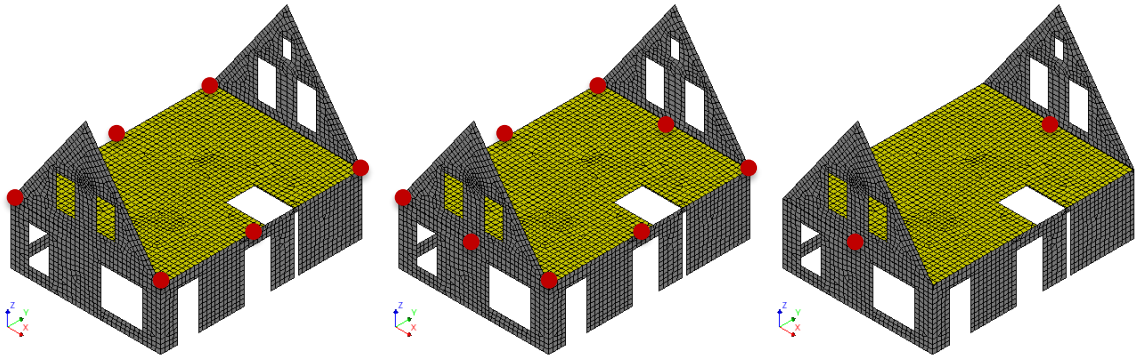

Figure 34. Location of output points for first floor: floor displacement (left), average storey displacement (middle), OOP displacement (right).

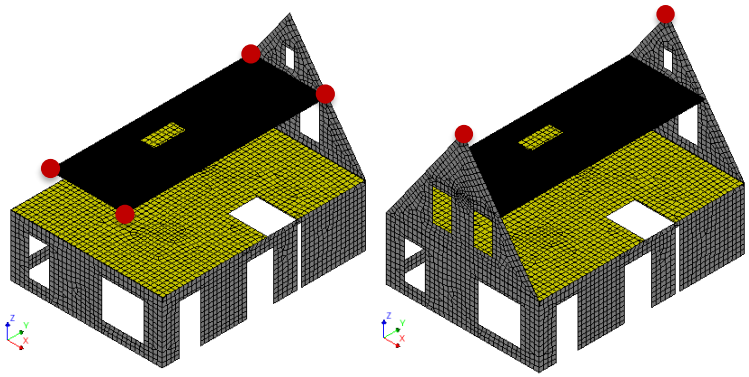

Figure 35. Location of output points: floor 2 (left), floor 3 (right).

The peak values of inter-storey floor displacements and drifts for both x and y directions are reported in Table 16 and

Table 17. Peak average storey displacement and OOP displacement are shown in Table 18.

Table 16. Inter-storey floor displacement NLTHA results for site-specific hazard.

GM ID	Peak I-S Displacement X Direction - mm			Peak I-S Displacement Y Direction - mm		
	Floor 1	Floor 2	Floor 3	Floor 1	Floor 2	Floor 3
1	1.06	0.25	0.13	0.42	2.83	3.55
2	1.39	0.37	0.05	0.55	3.03	3.42
3	1.54	0.39	0.09	0.53	3.17	4.26
4	0.91	0.22	0.10	0.37	2.21	2.52
5	1.16	0.32	0.10	0.36	2.55	2.71
6	1.16	0.36	0.09	0.46	2.61	3.22
7	1.20	0.11	0.11	0.54	3.63	3.65
8	1.74	0.11	0.22	0.53	3.62	4.49
9	1.15	0.29	0.07	0.50	3.14	3.29
10	1.14	0.18	0.08	0.40	2.82	2.76
11	1.22	0.21	0.10	0.47	2.96	3.67
Mean	**1.24**	**0.26**	**0.10**	**0.47**	**2.96**	**3.41**

Table 17. Inter-storey floor drift NLTHA results for site-specific hazard.

GM ID	Peak Drift X Direction - %			Peak Drift Y Direction - %		
	Floor 1	Floor 2	Floor 3	Floor 1	Floor 2	Floor 3
1	0.04	0.01	0.01	0.02	0.11	0.14
2	0.05	0.01	0.00	0.02	0.12	0.14
3	0.06	0.02	0.00	0.02	0.13	0.17
4	0.03	0.01	0.00	0.01	0.09	0.10
5	0.04	0.01	0.00	0.01	0.10	0.11
6	0.04	0.01	0.00	0.02	0.10	0.13
7	0.04	0.00	0.00	0.02	0.14	0.14
8	0.06	0.00	0.01	0.00	0.14	0.18
9	0.04	0.01	0.00	0.02	0.12	0.13
10	0.04	0.01	0.00	0.01	0.11	0.11

11	0.04	0.01	0.00	0.02	0.12	0.15
Mean	**0.05**	**0.01**	**0.00**	**0.02**	**0.12**	**0.14**

Table 18. Average storey displacement and OOP displacement NLTHA results for site-specific hazard.

GM ID	Peak Displacement X Direction - mm	Peak Displacement Y Direction - mm		
	AVG Storey 1	AVG Storey 1	OOP South	OOP North
1	1.07	1.68	12.95	0.44
2	1.39	3.93	31.05	0.58
3	1.55	5.04	38.24	0.55
4	0.92	2.13	15.54	0.38
5	1.17	2.16	16.54	0.38
6	1.18	2.01	16.32	0.50
7	1.20	2.87	22.35	0.57
8	1.72	3.70	26.28	0.61
9	1.14	3.07	22.01	0.55
10	1.13	3.33	24.62	0.45
11	1.21	3.22	23.02	0.50
Mean	**1.24**	**3.01**	**22.63**	**0.50**

4.1.3 Effective Height Drifts

The maximum drifts evaluated at the effective height of the building are listed for both the x- and y-direction in Table 19. The average storey drift is used.

Table 19. Peak effective height drift for NLTHA analyses for site-specific hazard.

GM ID	Peak Effective Height Drift X [%]	Peak Effective Height Drift Y [%]
1	0.04	0.06
2	0.05	0.14
3	0.06	0.18
4	0.03	0.08
5	0.04	0.08
6	0.04	0.07
7	0.04	0.11
8	0.06	0.14
9	0.04	0.11
10	0.04	0.12
11	0.04	0.12
Mean	**0.05**	**0.11**

4.1.4 Base Shear

Maximum reached base shear for both x and y direction is reported in Table 20. The governing mechanism is a two-way OOP bending failure at the first storey level of the South façade.

Table 20. Base shear NLTHA results for site-specific hazard.

GM ID	Governing Failure	Base Shear X [kN]	Base Shear Y [kN]
1	OOP South	+179.99 / -241.17	+187.82 / -180.11
2	OOP South	+238.50 / -254.90	+265.29 / -271.51
3	OOP South	+225.63 / -273.93	+232.44 / -258.36
4	OOP South	+152.20 / -243.76	+173.75 / -165.15
5	OOP South	+155.05 / -277.30	+168.51 / -162.67
6	OOP South	+166.28 / -251.25	+209.70 / -204.0
7	OOP South	+217.06 / -184.48	+199.50 / -235.47
8	OOP South	+255.14 / -239.34	+259.74 / -234.93
9	OOP South	+178.75 / -251.63	+200.32 / -222.53
10	OOP South	+198.46 / -212.63	+192.21 / -179.21
11	OOP South	+214.09 / -217.94	+234.46 / -217.29
Mean		**+198.29 / -240.76**	**+211.25 / -211.93**

4.1.5 Capacity Curves

The force-displacement curve of each ground motion are depicted in Figure 36. The displacement is recorded at the effective height location.

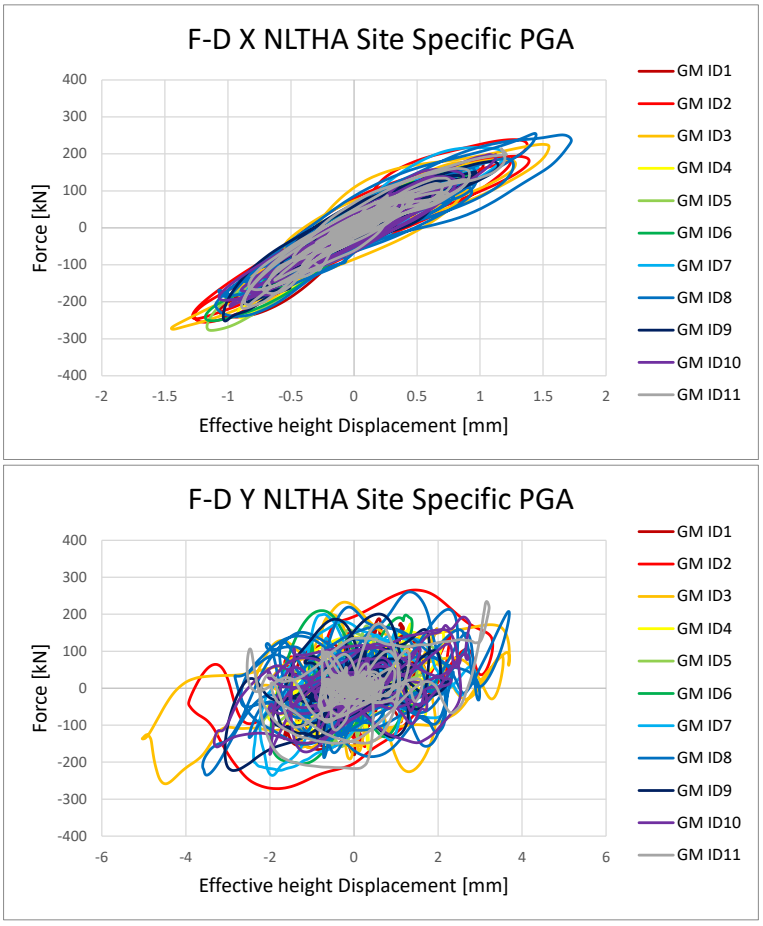

Figure 36. Capacity curves of each ground motion for site-specific hazard for X and Y direction.

4.2 Iterative Scaling of Input Ground Motion – Indirect Method

The original ground motions are amplified in order to evaluate the peak ground acceleration (PGA) that leads to failure (exceedance of the global drift limits), following an indirect method. The ground motions are scaled to a PGA of 0.35g.

The global failure mechanism is an OOP two-way bending at first floor level at the South façade. The average maximum inter-storey displacement in x direction recorded at the first floor location is 3.01 mm, equal to 0.11% of global drift. The average maximum inter-storey displacement in y direction recorded at the floor three location is 5.15 mm, equal to 0.20% of global drift. The average in-plane drift is below the drift limit calculated from normative. The average maximum OOP displacement in the South façade reaches 58.22 mm. Although analyses 6 and 7 do not reach 60 mm displacement in the South façade, a numerical collapse is obtained. GM ID 2 and 9 show, in addition to the OOP collapse, the one-way bending failure of the internal pier located at the second floor and connected to the North façade. The displacement in x direction reached at the top of the cantilever wall is above 60 mm for these two motions. Must be noted that the failure of the partition wall is not considered as global collapse. The average peak forces are equal to 305.5 kN in the positive direction and 365.3 kN for the negative direction in x. For the y direction the maximum forces in positive and negative direction are 346.6 kN and 343.9 kN.

4.2.1 Failure Mechanisms

The observed failure mechanism is a two-way OOP bending failure at the first storey level of the South façade. In addition, the partition wall connected to the North façade at the second floor collapse OOP in x direction in GM ID 2 and 9. A displacement limit of 60 mm is considered for the OOP failure. An example of failure mechanisms is shown below in Figure 37. Crack pattern of the different façades is depicted in Figure 38 Figure 39.

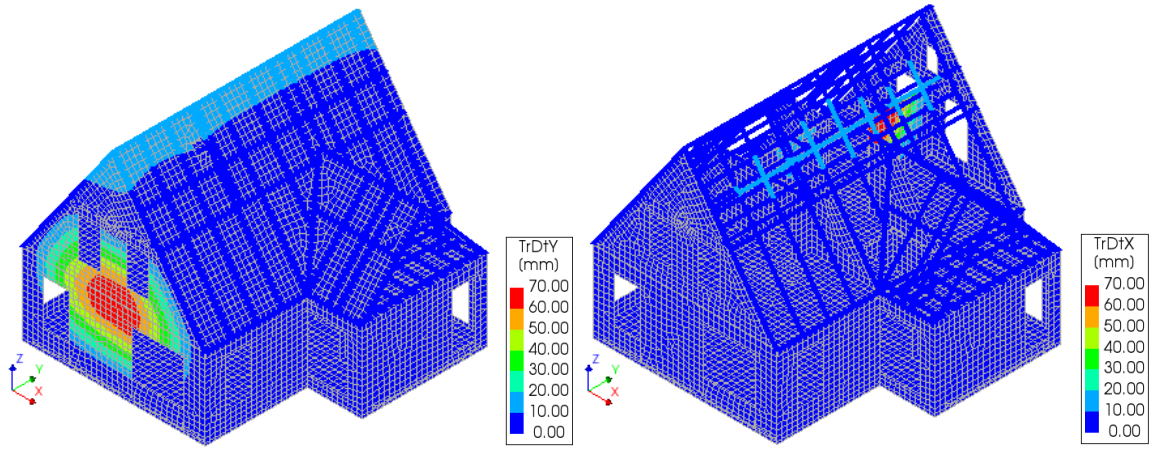

Figure 37. GM ID 2 for scaled PGA. Absolute maximum displacement in Y (left) and X (right) direction recorded during the entire motion.

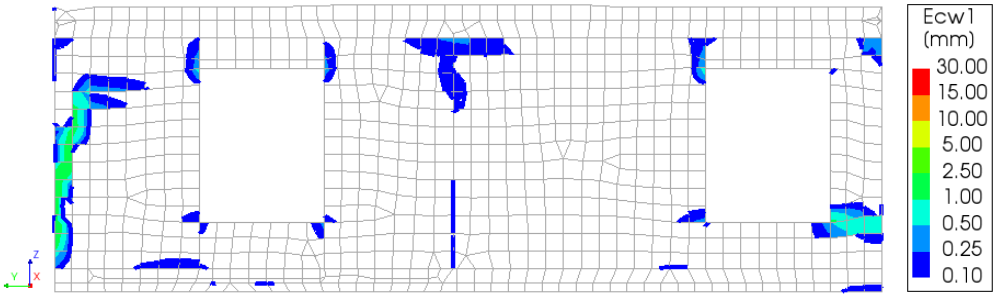

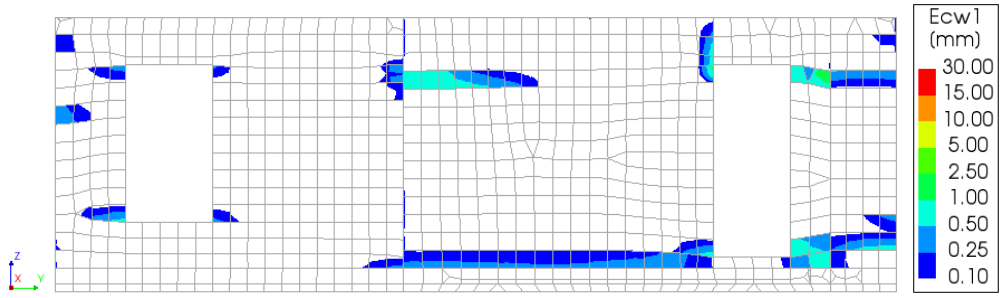

Figure 38. GM ID 2 for iterated PGA. Absolute maximum principal crack width recorded during the entire motion. West (top) and East (bottom) façade.

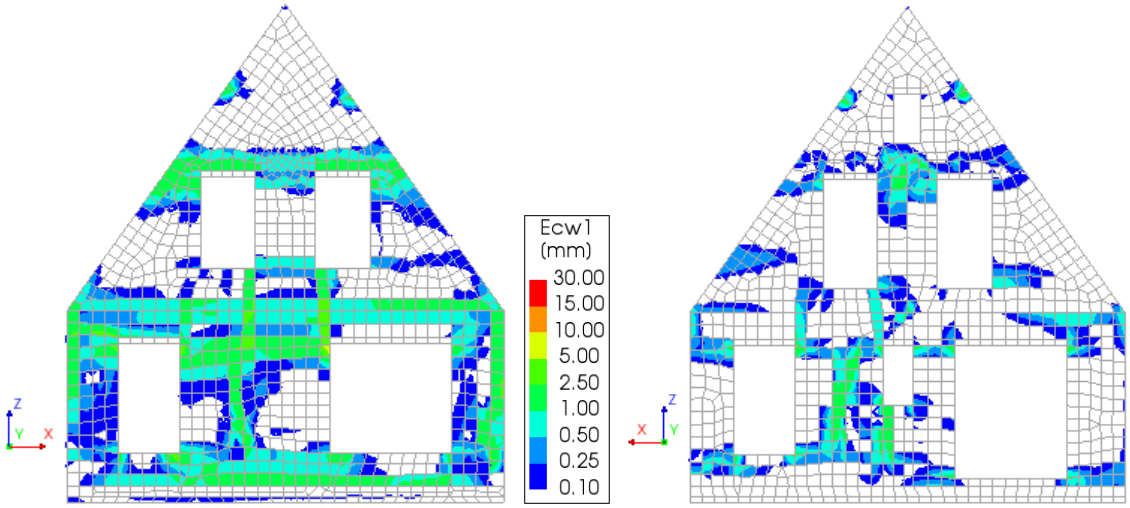

Figure 39. GM ID 2 for iterated PGA. Absolute maximum principal crack width recorded during the entire motion. South (left) and North (right) façade.

4.2.2 Inter-storey Drifts

As for the site-specific hazard, the peak values of the inter-storey displacements and drifts are divided in floor displacement, average storey and OOP displacement. Output point locations of the first floor are shown in Figure 34, while the output locations of timber floor and roof are shown in Figure 35 of previous section.

Peak values of floor displacement and drift for both x and y directions are reported in Table 21 and

Table 22. Peak average storey displacement and OOP displacement are shown in Table 23.

Table 21. Peak inter-storey floor displacement NLTHA results for a PGA of 0.35g.

GM ID	Peak Displacement X Direction - mm			Peak Displacement Y Direction - mm		
	Floor 1	Floor 2	Floor 3	Floor 1	Floor 2	Floor 3
1	2.19	0.62	0.18	0.72	3.01	3.45
2	4.09	0.39	0.29	1.03	4.43	5.98
3	2.68	0.90	0.19	0.75	4.09	6.01
4	2.00	0.44	0.19	0.71	3.86	4.29
5	2.80	0.67	0.26	0.66	4.24	4.93
6	2.48	0.89	0.17	0.88	4.81	5.87
7	2.73	0.49	0.24	0.87	3.13	2.88
8	3.00	0.47	0.29	0.75	5.12	5.85
9	2.82	0.84	0.13	0.91	5.44	5.17
10	3.41	0.23	0.42	0.78	5.50	5.48
11	4.89	0.98	0.47	1.13	4.58	6.79
Mean	**3.01**	**0.63**	**0.26**	**0.84**	**4.38**	**5.15**

Table 22. Peak inter-storey drift NLTHA results for a PGA of 0.35g.

GM ID	Peak Drift X Direction - %			Peak Drift Y Direction - %		
	Floor 1	Floor 2	Floor 3	Floor 1	Floor 2	Floor 3
1	0.08	0.02	0.01	0.03	0.12	0.14
2	0.15	0.02	0.01	0.04	0.18	0.24
3	0.10	0.04	0.01	0.03	0.16	0.24
4	0.07	0.02	0.01	0.03	0.15	0.17
5	0.10	0.03	0.01	0.02	0.17	0.20
6	0.09	0.04	0.01	0.03	0.19	0.23
7	0.10	0.02	0.01	0.03	0.12	0.11
8	0.11	0.02	0.01	0.03	0.20	0.23
9	0.10	0.03	0.01	0.03	0.22	0.20
10	0.13	0.01	0.02	0.03	0.22	0.22
11	0.18	0.04	0.02	0.04	0.18	0.27
Mean	**0.11**	**0.02**	**0.01**	**0.03**	**0.17**	**0.20**

Table 23. Average storey displacement and OOP displacement NLTHA results for a PGA of 0.35g.

GM ID	Peak Displacement X Direction - mm	Peak Displacement Y Direction - mm		
	AVG Storey 1	AVG Storey 1	OOP South	OOP North
1	2.24	6.77	50.75	0.77
2	4.16	8.83	69.99	1.11
3	2.71	9.12	73.84	0.81
4	2.02	4.04	34.53	0.74
5	2.83	4.15	34.47	0.86
6	2.57	5.25	46.64	0.95
7	2.78	5.58	45.46	0.94
8	3.03	7.75	65.40	0.91
9	2.85	5.55	43.60	1.01
10	3.44	10.02	82.11	0.85
11	5.02	11.65	93.61	1.20
Mean	**3.06**	**7.16**	**58.22**	**0.93**

4.2.3 Effective Height Drifts

The maximum drifts evaluated at the effective height of the building are listed in Table 24. The average storey drift value is used.

Table 24. Peak effective height drift for NLTHA analyses with a PGA of 0.35g.

GM ID	Peak Effective Height Drift X [%]	Peak Effective Height Drift Y [%]
1	0.08	0.25
2	0.15	0.32
3	0.10	0.33
4	0.07	0.15
5	0.10	0.15
6	0.09	0.19
7	0.10	0.20
8	0.11	0.28
9	0.10	0.20
10	0.13	0.37
11	0.18	0.43
Mean	**0.11**	**0.26**

4.2.4 Base Shear

Maximum reached base shear for both x and y direction is reported in Table 25. The governing mechanism is a two-way OOP bending failure at the first storey level of the South façade.

Table 25. Base shear NLTHA results for a PGA of 0.35g.

GM ID	Governing Failure	Base Shear X [kN]	Base Shear Y [kN]
1	OOP South	+242.20 / -380.04	+310.50 / -276.41
2	OOP South	+387.22 / -372.71	+464.45 / -454.01
3	OOP South	+289.79 / -357.54	+307.87 / -331.64
4	OOP South	+264.08 / -413.13	+305.68 / -298.14
5	OOP South	+283.04 / -472.23	+287.91 / -287.12
6	OOP South	+219.90 / -390.07	+398.91 / -354.85
7	OOP South	+348.19 / -198.27	+278.58 / -397.47
8	OOP South	+347.79 / -304.63	+354.89 / -307.99
9	OOP South	+265.47 / -400.72	+344.73 / -379.89
10	OOP South	+330.90 / -386.29	+329.82 / -304.69
11	OOP South	+381.54 / -342.76	+428.90 / -390.47
Mean		**+305.47 / -365.31**	**+346.57 / -343.88**

4.2.5 Capacity Curves

The force-displacement curve of each ground motion for both x and y direction are depicted in Figure 40. The displacement is recorded at the effective height location.

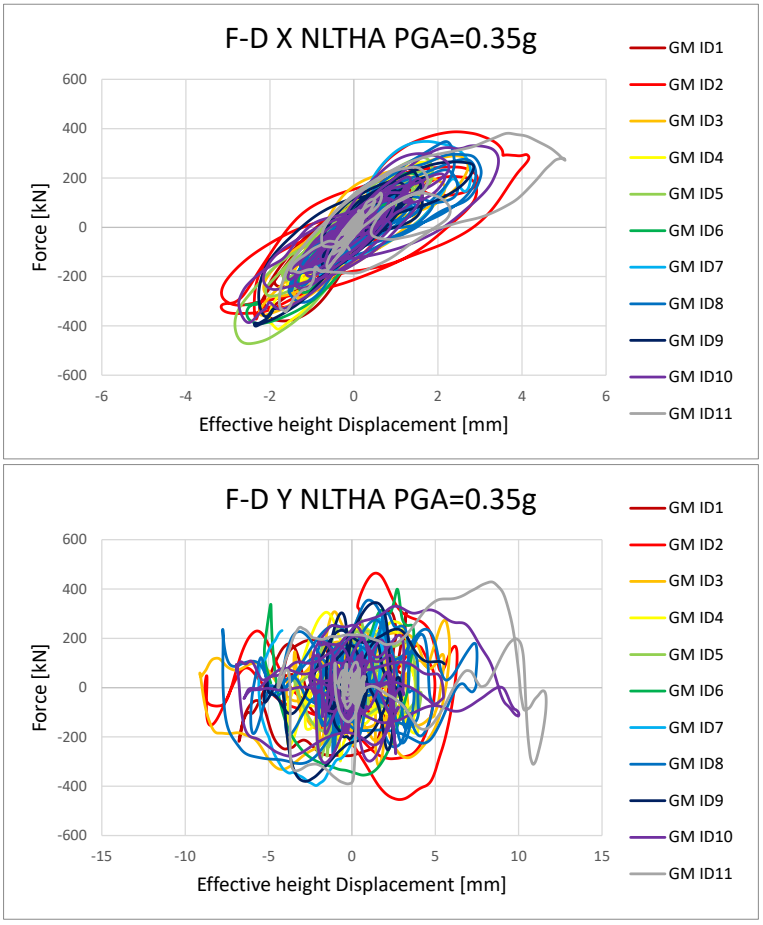

Figure 40. Capacity curves of each ground motion with PGA of 0.35g.

4.3 Comparison NLTHA-NLPO

A backbone curve is derived from the set of performed non-linear time history analyses in order to define an average global behaviour when the building is subjected to an dynamic ground motion. A maximum and a minimum force is extrapolated from each analysis and correlated with the corresponding maximum displacement. An average is made between for the data points from the site-specific hazard analyses. The same procedure is followed for the data points taken from the iterated NLTH analyses. A trilinear backbone curve is obtained and compared with the pushover capacity curves. For the x direction, the maximum positive force of the backbone curve is equal to 270.5 kN while the negative is equal to 375.7 kN at a displacement of 2.11 mm and 2.22 mm, respectively. The collapse displacement is computed by averaging the maximum displacement of the analyses which show collapse. The calculated collapse displacements are 3.67 mm for the positive direction and -2.30 mm for the negative direction, respectively. For the y direction, the maximum positive force of the backbone curve is equal to 312.2 kN while the negative is equal to 310.4 kN at a displacement of 4.25 mm and 4.84 mm, respectively. The collapse displacements are 8.27 mm for the positive direction and -7.41 mm for the negative direction, respectively.

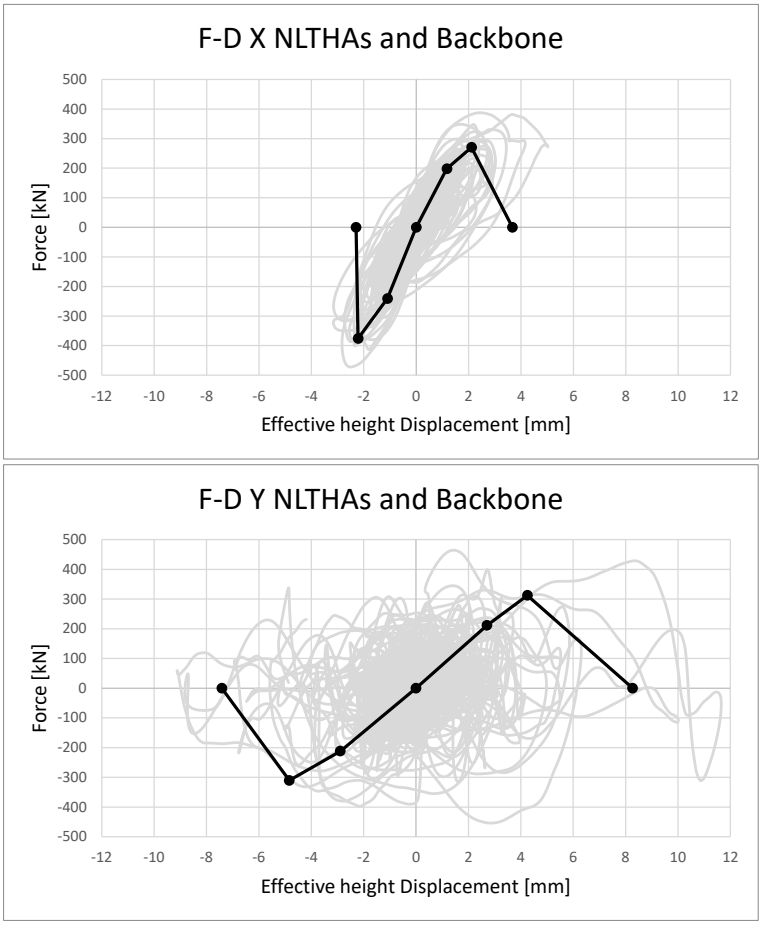

Figure 41. Backbone curves calculated from site-specific and iterated NLTHA analyses.

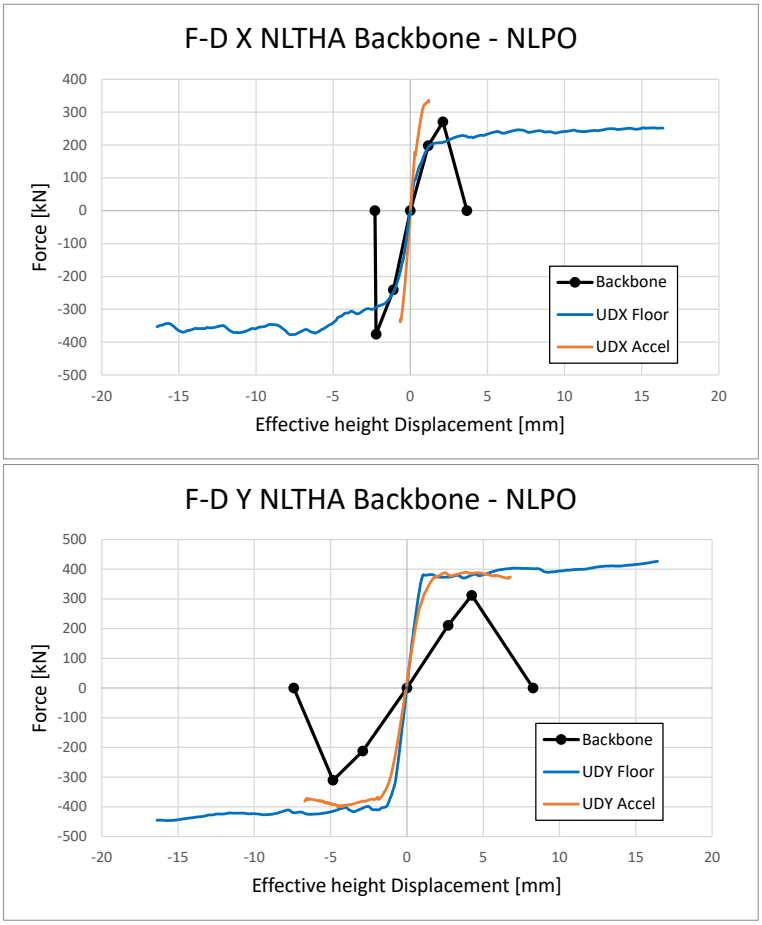

Figure 42. Backbone curve calculated from NLTHA analyses and comparison with NLPO curves.

Reference

[1] Schreppers et al. 2017 - DIANA FEA report 2016-DIANA-R1601 TU Delft Structural Mechanics CiTG report CM-2016-17, DIANA Validation report for Masonry modelling. 2016 DIANA FEA B.V.

[2] NEN (2018) - Assessment of the structural safety of buildings in case of erection, reconstruction, and disapproval - Induced earthquakes – Basis of design, actions and resistances. NPR9998:2018, NEN.

[3] NEN (2018) - Webtool NPR 9998: Bepaling van de seismische belasting. Available from URL: http://seismischekrachten.nen.nl/

[4] CVW (2018). "Applicatiedocument Beoordeling Seismische Capaciteit (ABSC)". CVW report no. CVW-ABSC-NPR2018-UK.

[5] Arup (2020) - NPR9998_Plan of Approach_Module 4 Phase 3_Rev.0.04, Arup (March, 2020).

Appendix A – Diana Modelling Approach

The modelling approach followed in the software Diana FEA 10.3 is described in the following tables.

Table 26. General modelling description

Input	Description
Analysis Software and Formulation	Diana FEA 10.3 – Implicit Solver
Overview of modelling approach	3D model – non-linear modelling; quadratic curved shell elements, class III beam elements, point interface used as elements. Non-linear pushover and non-linear transient dynamic analysis. Quadrilateral mesh 200x200 mm
Loads	Gravity, equivalent acceleration, modal pushover and base acceleration
Damping	2% Rayleigh Damping

Table 27. Masonry model overview

Input	Description
Element Formulation	Quadratic curved shell elements (CQ40S, CT30S). Full integration scheme 3x3 in the plane and 3 integration points in the thickness of longitudinal façades and 7 integration points in the thickness of transversal façades. Extra dynamic mass to account for veneer, chimney
Material Type	Engineering Masonry Model accounting for cracking, shearing and crushing behaviour. Failure located in integrations point in 4 different directions, horizontal, vertical and two diagonal

Table 28. Timber roof model overview

Input	Description
Element Formulation	Quadratic curved shell elements (CQ40S). Full integration scheme 3x3 in the plane and 3 integration points in the thickness
Material Type	Linear elastic orthotropic material

Table 29. Timber model overview

Input	Description
Element Formulation	Class III beam elements (CL18B). Three integration points in the length
Material Type	Linear elastic isotropic material

Table 30. Interface model overview

Input	Description
Element Formulation	Point interface elements (N6IF)
Material Type	Coulomb friction material

Table 31. Concrete model overview

Input	Description
Element Formulation	Quadratic curved shell elements (CQ40S). Full integration scheme 3x3 in the plane and 3 integration points in the thickness
Material Type	Total Strain Rotating Crack Model

Table 32. Concrete model overview

Input	Description
Element Formulation	Quadratic curved shell elements (CQ40S). Full integration scheme 3x3 in the plane and 3 integration points in the thickness
Material Type	Total Strain Rotating Crack Model

Table 33. Reinforcement model overview

Input	Description
Element Formulation	Distributed grid reinforcement which automatically accounts for bar diameter in the two directions, spacing and concrete cover. Bar reinforcements modelled explicitly for webs of ground floor
Material Type	Von Mises plasticity

Appendix B – Detailed Analysis Results for GM ID 9 Site-Specific Hazard

Table 34. Results overview of GM ID 9 site-specific hazard.

GM ID 9 - Data	Value
Peak IS Displacement X Direction Floor 1 - mm	1.15
Peak IS Displacement X Direction Floor 2 - mm	0.29
Peak IS Displacement X Direction Floor 3 - mm	0.07
Peak IS Displacement Y Direction Floor 1 - mm	0.50
Peak IS Displacement Y Direction Floor 2 - mm	3.14
Peak IS Displacement Y Direction Floor 3 - mm	3.29
Peak IS Drift X Direction Floor 1 - %	0.04
Peak IS Drift X Direction Floor 2 - %	0.01
Peak IS Drift X Direction Floor 3 - %	0.00
Peak IS Drift Y Direction Floor 1 - %	0.02
Peak IS Drift Y Direction Floor 2 - %	0.12
Peak IS Drift Y Direction Floor 3 - %	0.13
Peak Effective Height Drift X [%]	0.04
Peak Effective Height Drift Y [%]	0.02
Base Shear X [kN]	+178.75 / -251.63
Base Shear Y [kN]	+200.32 / -222.53

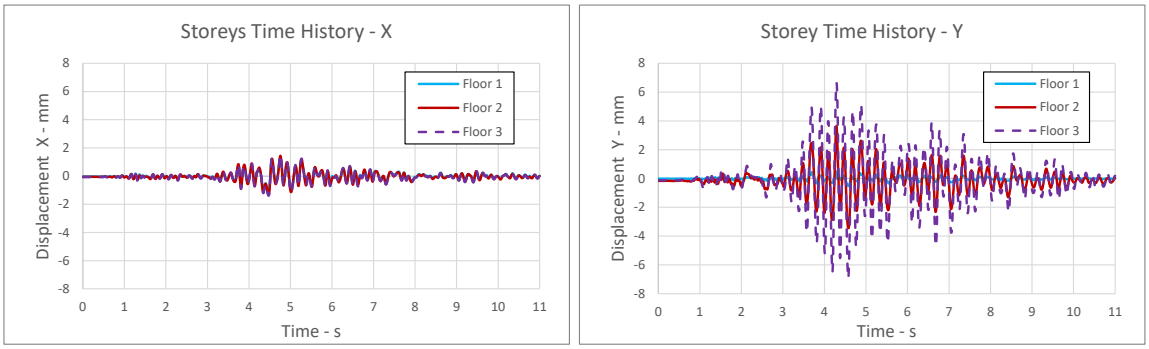

Figure 43. Inter-storey drift time histories in direction X and Y.

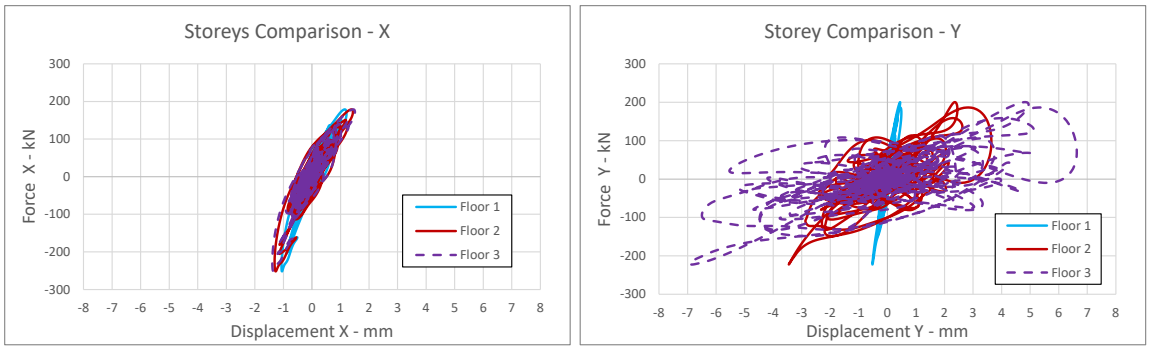

Figure 44. Force-Displacement of different storeys in direction X and Y.

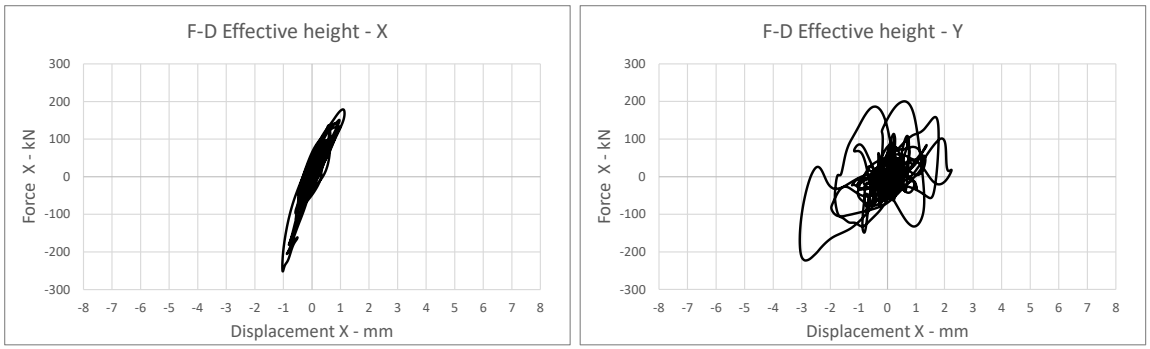

Figure 45. Force-Displacement at effective height in direction X and Y.

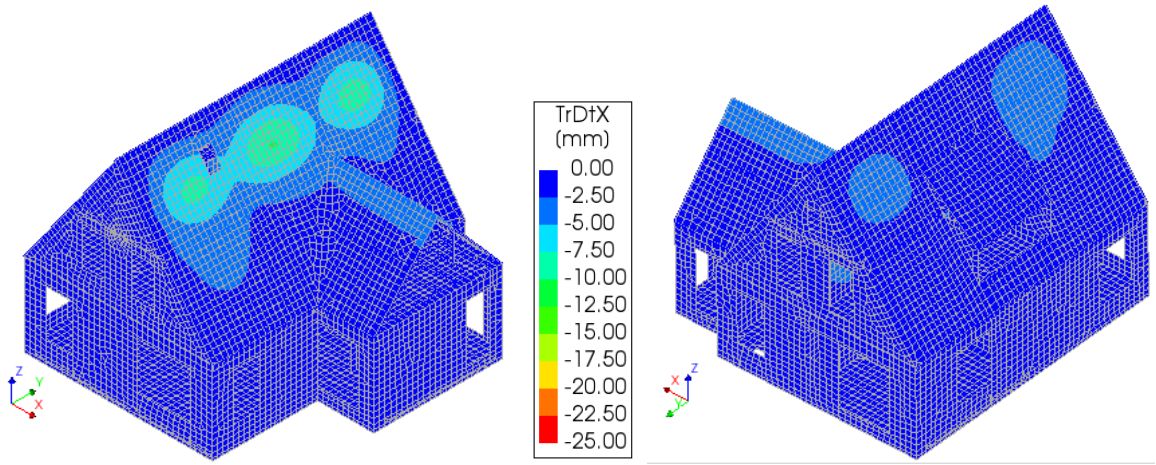

Figure 46. External walls absolute maximum displacement in X direction. South-East and North-West view.

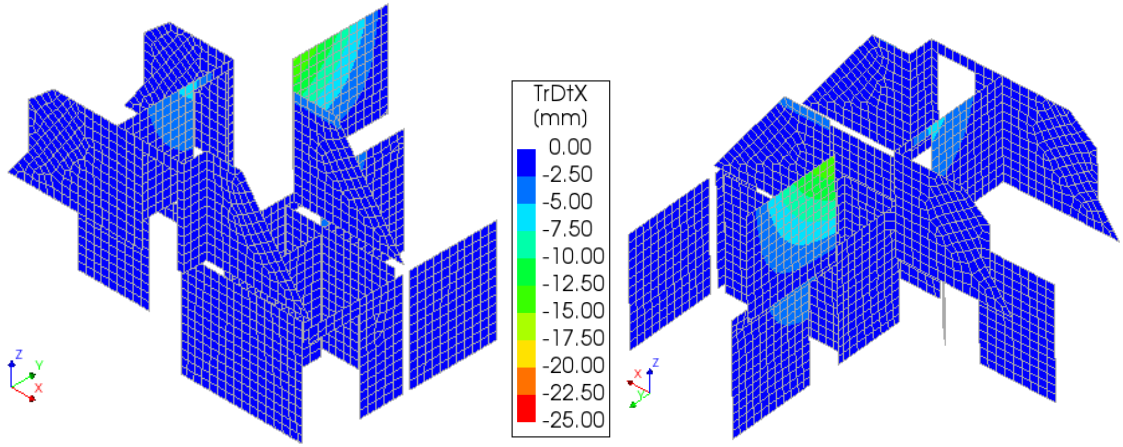

Figure 47. Internal walls absolute maximum displacement in X direction. South-East and North-West view.

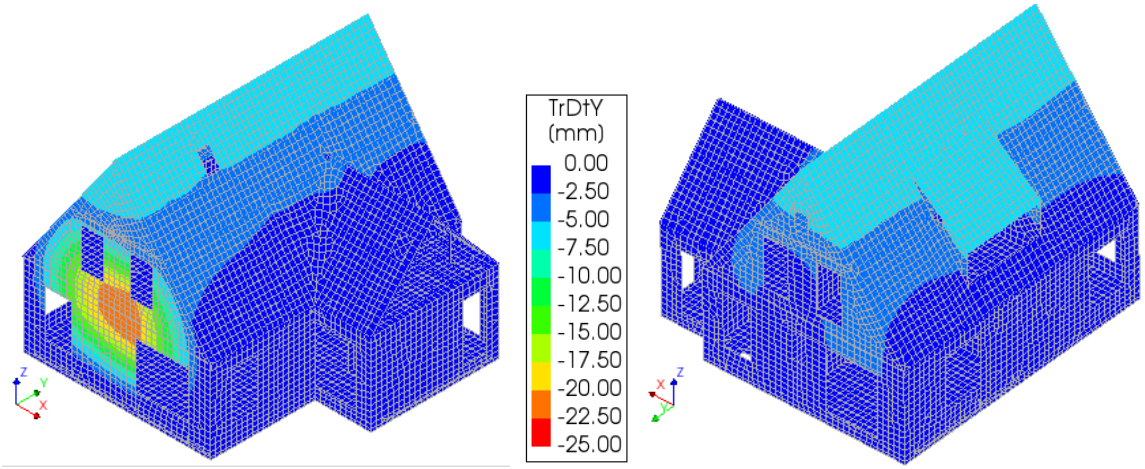

Figure 48. External walls absolute maximum displacement in Y direction. South-East and North-West view.

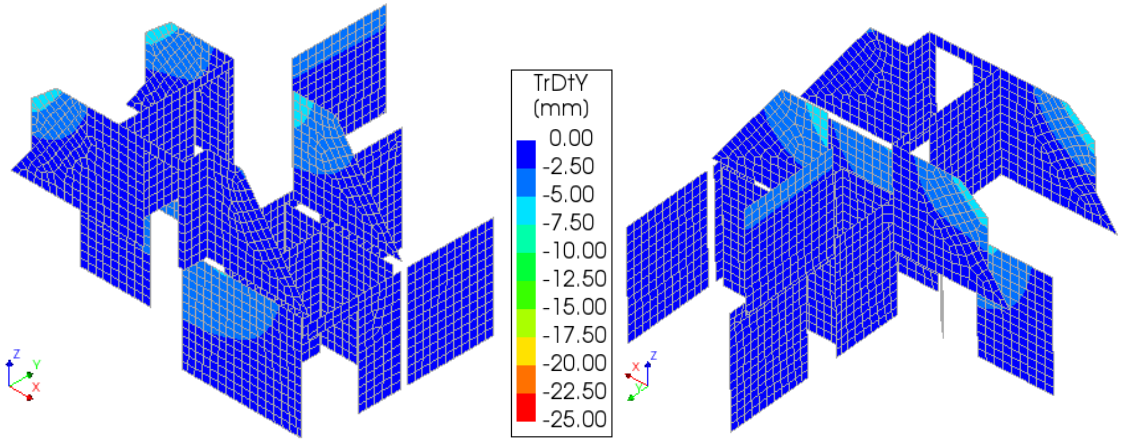

Figure 49. Internal walls absolute maximum displacement in Y direction. South-East and North-West view.

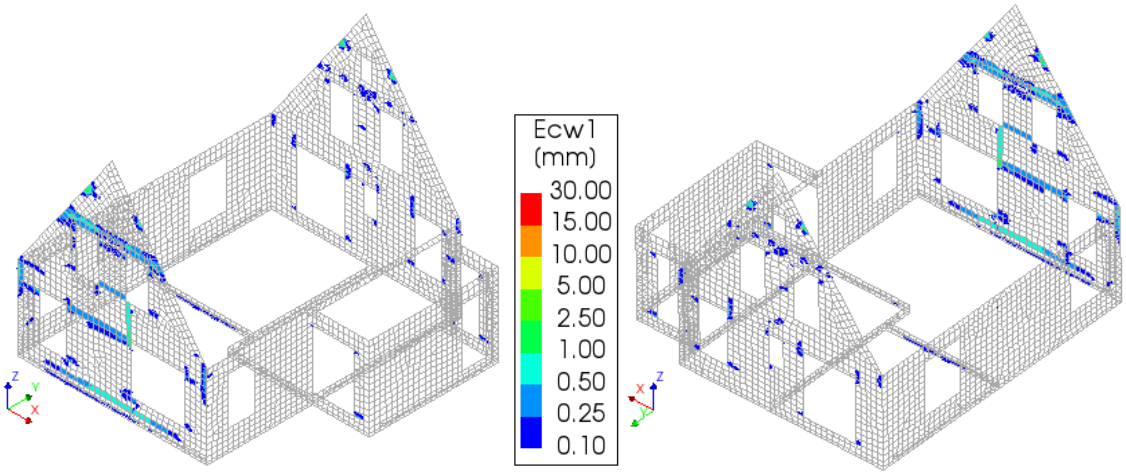

Figure 50. Max recorded principal crack width of external walls. South-East and North-West view.

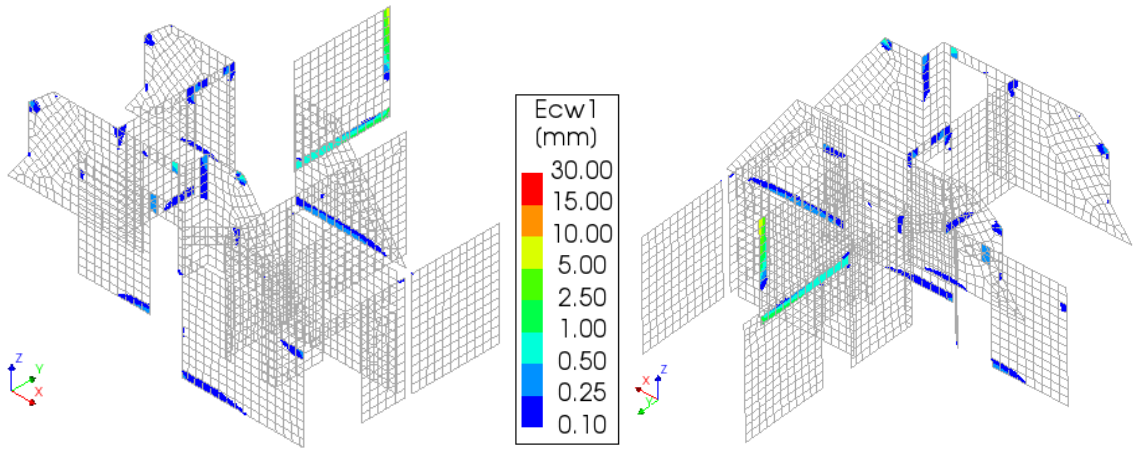

Figure 51. Max recorded principal crack width of internal walls. South-East and North-West view.

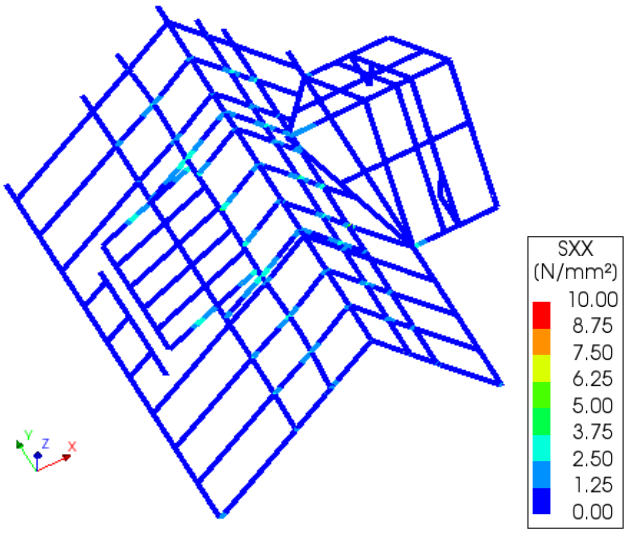

Figure 52. Peak of global X stress of roof beams.

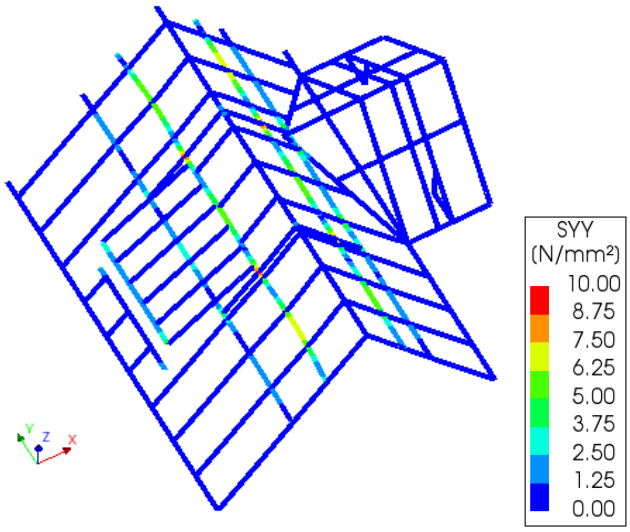

Figure 53. Peak of global Y stress of roof beams.

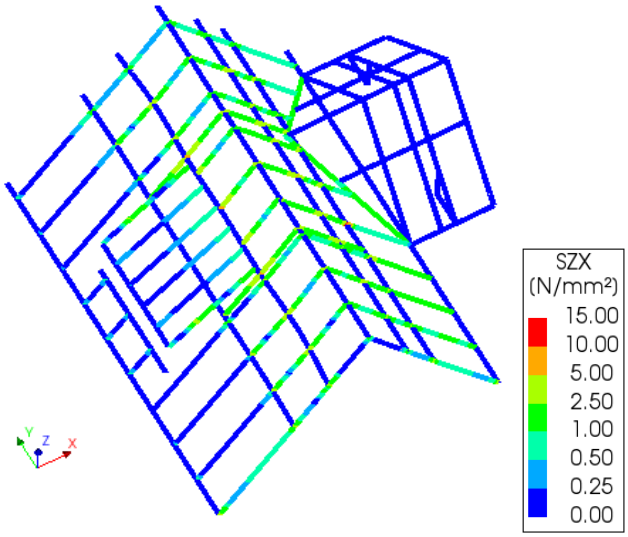

Figure 54. Peak of global ZX shear stress of roof beams.

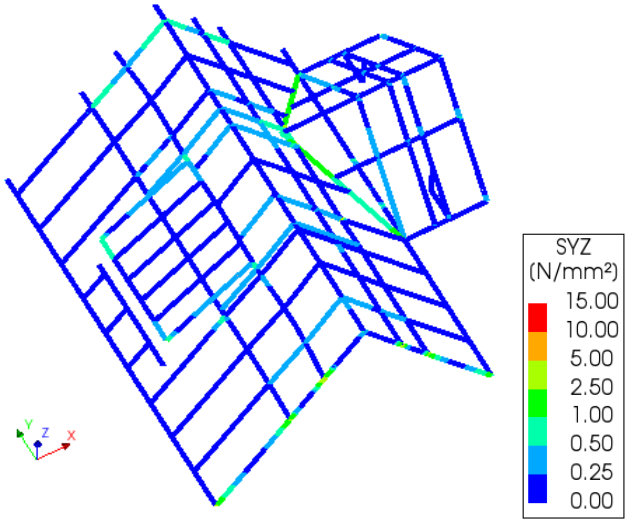

Figure 55. Peak shear stress YZ of roof diaphragm.

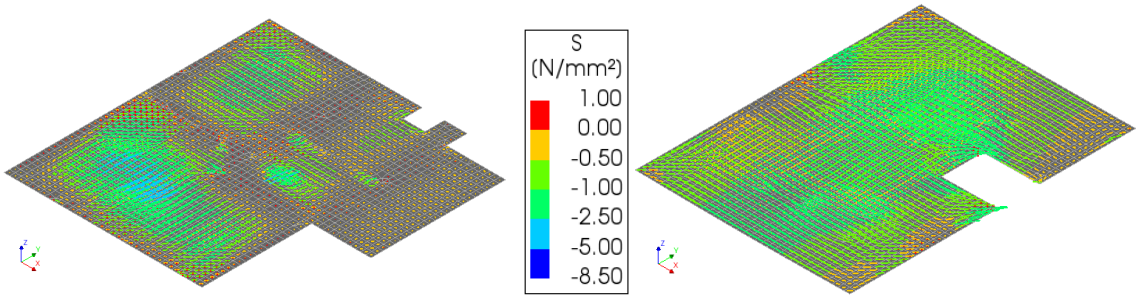

Figure 56. Peak principal compressive stress at bottom of concrete floors – Layer 1. Ground PS Isolatievloer (left) and first floor hollow-core slab (right).

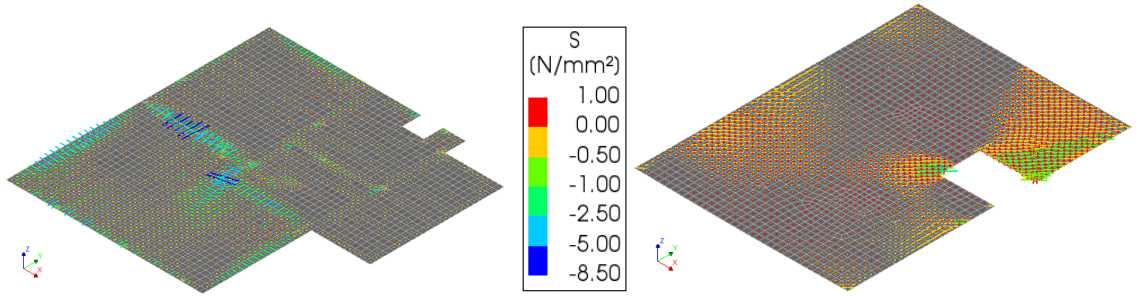

Figure 57. Peak principal compressive stress at top of concrete floors – Layer 7. Ground PS Isolatievloer (left) and first floor hollow-core slab (right).

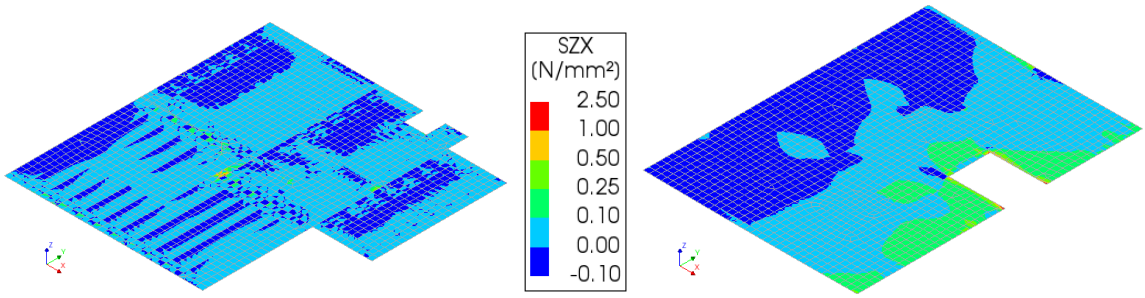

Figure 58. Peak shear stress XZ of concrete floors. Ground PS Isolatievloer (left) and first floor hollow-core slab (right).

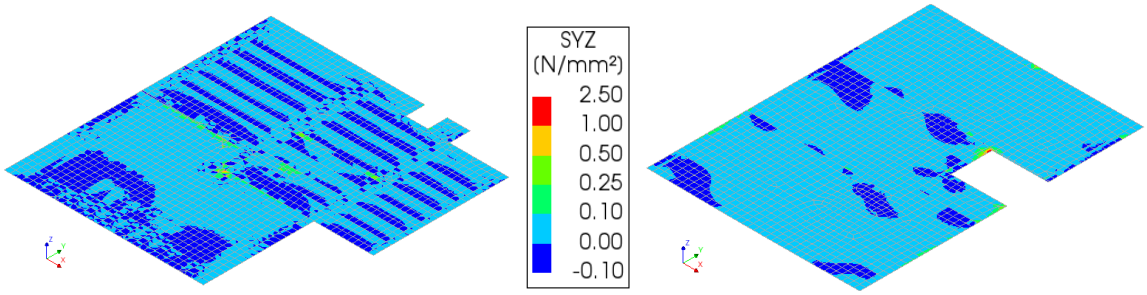

Figure 59. Peak shear stress YZ of concrete floors. Ground PS Isolatievloer (left) and first floor hollow-core slab (right).